Quantification of Land-Atmosphere Coupling and Implications for Drought Persistence In Observations and Model Simulations of 20th Century Climate and 21st Century Climate Change

by

Erica E. Bickford

A thesis submitted in partial fulfillment of the requirements for the degree of

Master of Science

(Atmospheric and Oceanic Sciences)

at the

UNIVERSITY OF WISCONSIN-MADISON

2008

ABSTRACT

Of all recurring natural disasters, long-term drought is one of the most devastating and costly due to large spatial extent and often long duration. The mechanisms responsible for the maintenance of long-term droughts are not well understood, however many drought analyses allege the importance of land-atmosphere feedbacks and speculate that these feedbacks will amplify changes in the hydrological cycle in the presence of climate change, increasing drought severity. A statistical lagged correlation method is applied to IPPC model and observed precipitation and evaporation data to quantify JJA land-atmosphere coupling based on a positive feedback between evaporation and later precipitation. Results of this statistical method are broadly consistent with results of other land-atmosphere coupling analyses with some important differences, most notably in the Sahara and Arabian deserts. In addition, drought analysis is conducted using a percentile scheme to quantify JJA drought frequency and drought persistence. The relationship between land-atmosphere coupling and drought persistence is analyzed by plotting drought persistence against land-atmosphere coupling; the result shows a positive linear relationship in three regions examined in which model drought persistence increases with land-atmosphere coupling strength. Enabled with this relationship for 20th century model data, we examine drought in IPCC simulations of 21st century climate to determine if land-atmosphere coupling is strongly correlated with increasing drought frequency. Surprisingly, no significant relationship is found, indicating that land-atmosphere coupling does not contribute strongly to future drought as many previous studies have suggested, and that other, more large-scale climate processes—poleward shifts in stormtracks, and changes in land-ocean temperature contrasts—are primarily responsible for changes in hydrological extremes in climate change simulations.

ACKNOWLEDGEMENTS

First and foremost, I would like to thank and acknowledge the contributions of Dr. Dave Lorenz to this research. In many ways the work presented in this thesis builds on a conceptual and analytical framework developed by Dave. In addition, his technical assistance with data processing, analytical guidance, and direction in statistical analyses were instrumental to the successful completion of this project.

I also thank my academic and research advisor, Dr. Eric DeWeaver for guiding this research project and its formulation into a Master's thesis. Working with Eric over the past two and a half years has made me a better analytical thinker and a better scientist. Approaching climatological research from a physical, rather than biological perspective was challenging and I appreciate that Eric always made himself available to discuss my uncertainties—often for hours at a time—lending his invaluable expertise to the theoretical and analytical dimensions of this research.

For taking time out of their busy end-of-semester schedules to read, approve and provide constructive feedback for this thesis, I thank my thesis readers; Dr. Eric DeWeaver, Dr. Dan Vimont and Dr. Ankur Desai.

Finally, I thank the National Science Foundation for supporting this work (grant no. #144QR) as part of the Drought in Coupled Models Project (DRICOMP) under Eric DeWeaver and Dave Lorenz.

TABLE OF CONTENTS

LIST OF FIGURES

LIST OF TABLES

CHAPTER ONE: INTRODUCTION AND MOTIVATION

In the early the 21st century, effects of climate warming have already begun to be observed, fostering broader awareness and a growing need to incorporate climate science into mitigation and adaptation strategies for areas sensitive to projected effects of climate change. The Intergovernmental Panel on Climate Change's (IPCC) Fourth Assessment Report (AR4) Working Group I (WGI) assesses the physical science of climate change. In their summary for policymakers, the WGI reports that observed long-term changes associated with warming

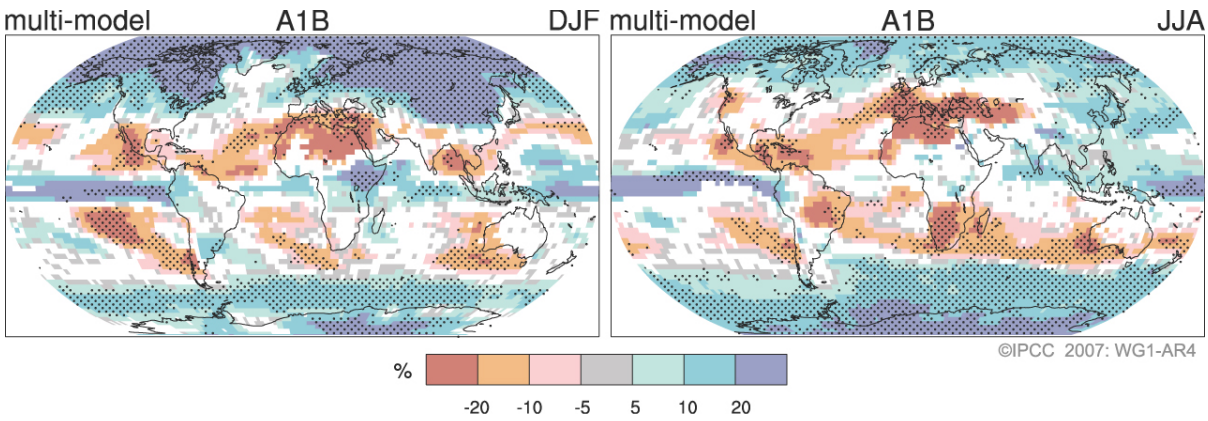

Fig. 1.1. *Changes in precipitation (in percent) for the period 2090-2099, relative to 1980-1999. Values are multi-model averages based on the SRES A1B scenario for DJF (left) and JJA (right). White areas are where less than 66% of the models agree in the sign of the change and stippled areas are where more than 90% of the models agree on the sign of the change (IPCC, 2007a).*

climate include changes in arctic sea ice, precipitation, wind patterns and extreme weather including heavy precipitation, intensified tropical cyclones, heat waves and droughts (IPCC, 2007a). Figure 1.1 illustrates the WGI's projection for future precipitation changes during boreal winter (DFJ=December, January and February) and summer (JJA=June, July and August), respectively. Changing precipitation patterns are of particular concern both for regions subject to extreme precipitation and floods, and those prone to water shortages and droughts.

1.1 INCREASED DROUGHTS AND ARIDITY

The IPCC's Working Group II (WGII) assesses impacts, adaptation and vulnerabilities associated with climate change. In their summary for policy makers, the WGII expects drought-affected areas to expand, identifying Africa, Asia, Europe, Latin America and North America as regions sensitive to increasing drought due to water resources stress, proliferation of drought-related disease, escalating heat waves, regime-shifts in vegetation and competition for over-allocated water resources (IPCC, 2007b).

The hydrological impacts of climate change are of particular interest to states and communities in America's West and Southwest that rely on the Colorado River as their primary water source (Barnett and Pierce, 2008). In recent years, several scientific studies

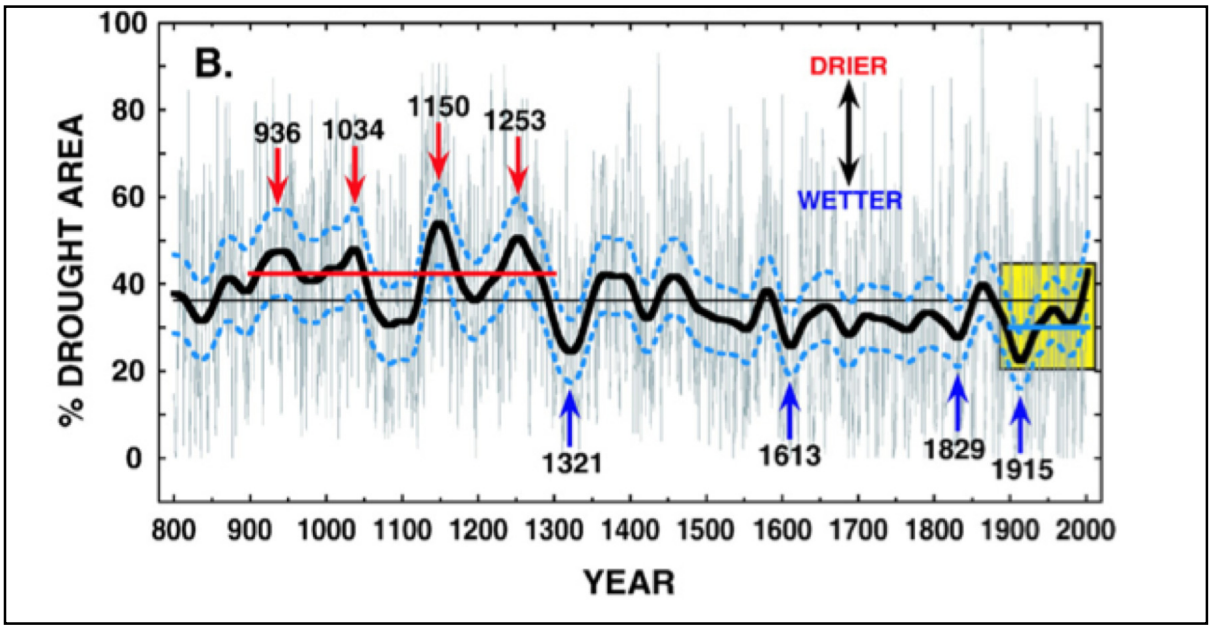

Fig. 1.2. *Long-term aridity changes in western North America from Cook et al. (2007) using a Drought Area Index (DAI) calculated from tree-ring records. The four driest (red) and four wettest (blue) epochs are marked with arrows. Dashed blue lines mark the 95% confidence interval; the thin black line is the long-term mean; and the yellow box encompasses the 20th century through 2003. Historical records indicate that the region is capable of droughts of far greater severity than observed during the 20th century, and that the most recent trend is one of increasing aridity (Cook et al., 2007).*

have investigated the occurrence of drought in North America. Cook et al. (2004) used centuries long, annually resolved tree-ring records to generate a gridded network of drought reconstructions over a large portion of North America and found that the Western U.S. (including parts of Northern Mexico and Southern Canada) has historically experienced far greater droughts than observed in the current century (see Fig. 1.2). This suggests that even without the influence of anthropogenic climate change, this region is predisposed to transition toward a more arid climate in response to warmer temperatures—and therefore particularly vulnerable to reductions in precipitation leading to long-term droughts.

Seager et al. (2007) also examined possible future shifts to arid climates in Southwestern North America through analysis of time histories for precipitation produced by IPCC AR4 climate model simulations of anthropogenic climate change. Results showed a broad consensus among models that the region would become drier in the 21st century (see Fig. 1.3) and that the levels of aridity experienced during the most severe droughts of the 20th century would become the new climatology for the region (Seager et al., 2007). As evident in Figure 1.3, however, there is a significant amount of uncertainty among models forecasting future precipitation and, by extension, future drought.

Concerns of increased drought under a warming climate are not limited to North America. The Mediterranean is one of the most responsive regions to climate change evidenced by "pronounced warming" and significant decreases in spring and summer precipitation leading to regime shifts toward more arid climates—similar to the American Southwest (Gao and Giorgi, 2008). The African Sahel (see Fig. 2.3), on the edge of the Sahara desert, is also susceptible to severe droughts and has experienced acute drying in the latter half of the 20th century (Biasutti and Giannini, 2006; Foley et al., 2003). Biasutti and

Giannini (2006) found reflective Northern Hemisphere sulfate aerosols forcing a sea surface temperature (SST) gradient in the Atlantic to be responsible for historical Sahel precipitation variability and drying—however cross-model consensus for this mechanism broke down when forecasting future precipitation. Foley et al. (2003), by comparison, classified the unusually persistent long-term droughts in the Sahel as regime shifts, triggered by some large-scale climate forcing and maintained by strong feedbacks between vegetation and the atmosphere via radiative energy and water balance. These studies illustrate that identifying and understanding mechanisms responsible for triggering and maintaining droughts is essential to forecasting the effects of climate change on future drought occurrence.

1.2 PREDICTING FUTURE DROUGHT

Of all recurring natural disasters, prolonged drought is one of the most devastating and costly, due to a wide spatial extent and often long duration (Sheffield and Wood, 2008; Cook et al, 2007; Herweijer et al., 2007). The ability to reliably predict the location, duration, severity and frequency of future drought would be extremely valuable, and vital, to governments and desert communities developing drought plans (Goodrich and Ellis, 2008) and preparing for future water shortages (Balling and Gober, 2007; Barnett and Pierce, 2008).

Extensive analysis has been conducted on severe or long-term droughts occurring during the 20th century, particularly the 12-year "Dustbowl" drought in the Great Plains of North America during the 1930's (Narisma et al., 2007; Schubert et al., 2004a; Alley et al., 2003), the 11-year 1950's drought in the Southwestern U.S. (Cook et al., 2007; Schubert et al., 2004b), the 30-year drought in the African Sahel (Narisma et al., 2007; Foley et al.,

2003), the 1988 drought in the western U.S. (Trenberth et al., 1988) and the recent 6-year drought over the western U.S. (Cook et al, 2007). As a region evidently prone to drought, the western U.S.—particularly the Great Plains—has been an area of special consideration for scientific research. Several studies using a variety of methods have found that the most significant climatic feature associated with—and the apparent cause of—drought in this region are sea surface temperatures (SSTs) in the Tropical Pacific (Cook et al, 2007; Herjweijer et al., 2007; Schubert et al., 2004a, 2004b; Trenberth et al., 1988). Trenberth et al., (1988) linked the 1988 drought to the 1986-1987 El Niño in the Tropical Pacific. Schubert et al. (2004b) however, identified the 1930's period as distinctly lacking in El Niño Southern Oscillation (ENSO) activity and not a likely mechanism for maintaining a multi-year drought—although they did conclude that Tropical Pacific SSTs account for as much as

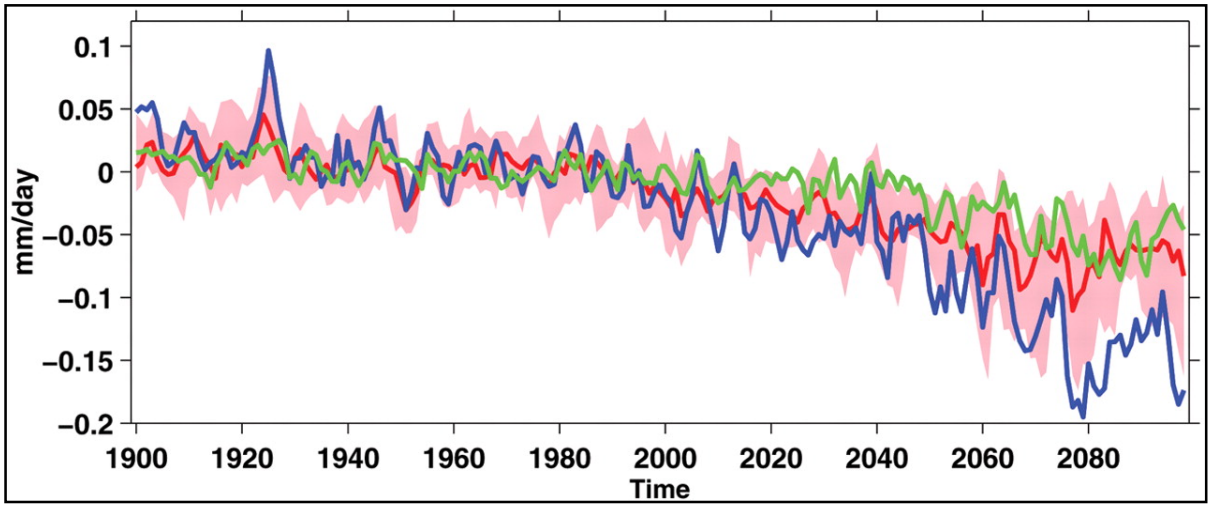

Fig. 1.3. *Modeled changes in the difference between annual mean precipitation and evaporation (P-E) over the American Southwest from Seager et al. (2007). Future projections use the SRES A1B emissions scenario. The pink region indicates the 25th-75th percentiles of the 19-model P-E distribution, the red line is the median, the blue line is the ensemble mean of P and the green line is the ensemble mean of E. Model results indicate a large amount of uncertainty in future precipitation over the Southwest, yet a generally decreasing trend (Seager et al., 2007).*

one third of low frequency variability in Great Plains precipitation. Sea surface temperature gradients have also been attributed to long-term drought in the Sahel (Biasutti and Giannini, 2006; Schubert et al., 2004a). Other studies have found a strong forcing connection between anomalously cool, La Nina-like SSTs in the Tropical Pacific and drought in the Great Plains (Cook et al., 2007; Herweijer et al., 2007; Schubert et al., 2004a). These same studies also concede, that while SST may be the climatic forcing triggering drought, it is *not the mechanism* controlling severity, or maintaining persistence over several years. This secondary drought forcing is attributed to positive feedbacks between vegetation and climate (Narisma et al. 2007), or land-surface and atmosphere where soil moisture acts as a reservoir for low-frequency precipitation anomalies (Schubert et al., 2004a, 2004b; Trenberth et al., 1988).

This depiction of long-term drought forcings satisfies the requirements of Alley et al. (2003) for abrupt climate change. They, and others (Narisma et al., 2007; Foley et al., 2003) identify both the Dustbowl and Sahel droughts as abrupt climate change events, requiring a trigger, an amplifier and a globalizer (Alley et al., 2003). If, as suggested, positive feedbacks between the land-surface and atmosphere serve as this amplifying feature and are responsible for maintaining droughts over many years, the study of these feedbacks will be just as important for future drought prediction as the effect of increasing greenhouse gases on SSTs in that the potential for more droughts and more severe droughts will be compounded by these positive feedbacks (Sheffield and Wood, 2008).

Several studies have endeavored to use climate models forced with projected emissions scenarios to predict the extent and severity of future drought (Sheffield and Wood, 2008; Burke and Brown, 2007; Burke at al., 2006; Rowell and Jones, 2006). Many

uncertainties accompany these analyses due to their use of model derived climate variables, such as soil moisture, that lack adequate observations to be verified against (Burke and Brown, 2007). Nevertheless, all studies report some measure of increased drought in addition to increases in drought severity (Burke and Brown, 2007), and frequency of long-term droughts, though there is significant spread among model simulations possibly due to differences in land-atmosphere interactions within the models (Sheffield and Wood, 2007; Rowell and Jones, 2006). The uncertainties associated with future drought prediction coupled with potentially important secondary forcings from land-atmosphere interactions (in this paper referred to as "land-atmosphere coupling") reveal the need to better understand land-atmosphere interactions in both climate models and observations, their connection to long-term droughts, and their role in future drought persistence.

This research presents a statistical method for quantifying land-atmosphere coupling that is applied to both climate models and observations, and linearly regressed against a drought persistence parameter calculated from model precipitation data to determine the relationship between land-atmosphere interactions and 20th century drought persistence within the models. This measure of land-atmosphere coupling is then compared to projections of future drought to determine whether, as other studies have suggested, regions of strong land-atmosphere coupling will be more susceptible to persistent drought as a result of positive feedbacks amplifying effects of large-scale drought forcings.

The remainder of the thesis is laid out as follows; Chapter 2 summarizes the relevant literature to provide a background on the state of the science of land-atmosphere coupling, Chapter 3 includes the methods, results and discussion of a land-atmosphere coupling statistic introduced in this study, Chapter 4 includes the methods, results and discussion of

drought persistence for the 20th century. Chapter five compares the findings of the land-atmosphere coupling analysis in Chapter 3 to findings of the drought persistence analysis in Chapter 4 to determine the extent to which drought persistence can be inferred from the strength of land-atmosphere coupling. Chapter 6 examines the results of Chapter 3 as they relate to 21st century drought persistence and Chapter 7 presents a summary and major conclusions from the research.

CHAPTER TWO: BACKGROUND

The influence of land-atmosphere interactions on climate processes has gained a growing amount of attention from the climate science community in recent years, yet the concept of land-surface processes affecting hydroclimate variability is not an altogether new idea. As early as 1880 Aughey is quoted describing a positive soil-atmosphere feedback in Nebraska:

> "It is the great increase in absorptive power of the soil, wrought by cultivation, that has caused and continues to cause an increasing rainfall in the state…After the soil is broken, a rain as it falls is absorbed by the soil like a huge sponge. The soil gives this absorbed moisture slowly back to the atmosphere by evaporation. Thus year-by-year as cultivation of the soil is extended, more of the rain that falls is absorbed and retained to be given off by evaporation, or to produce springs. This, of course, must give increasing moisture and rainfall" (USDA, 2004).

Others generated similar conclusions, yet until the later part of this century there was a distinct lack of observations with which to test these hypotheses. Even now, verification of land-atmosphere coupling in nature is limited by insufficient availability of observational data on a global scale—a subject discussed more in the chapters that follow.

2.1 LAND-ATMOSPHERE COUPLING: A MODEL EXPERIMENT APPROACH

Eltahir (1998) claims to be the first to present a hypothetical pathway connecting soil moisture conditions with successive precipitation *and* test that hypothesis using observations and numerical experiments (Zheng and Eltahir, 1998). His proposed mechanism focused on radiative feedbacks induced by anomalously wet soil moisture increasing net radiation at the surface and the total heat flux from the surface into the atmosphere, enhancing moist static energy in the boundary layer. Increased moist static energy amplifies the frequency and magnitude of local convection and strengthens large-scale circulation leading to more rainfall. This hypothesis was tested using observations from Kansas collected during the

First ISLSCP Field Experiment (FIFE), which supported the overall feedback process but could not be used to prove the mechanistic pathways. The observations did, however, reveal the functional feedback similarities between vegetation and soil moisture with each feature influencing radiative and hydrological surface processes (Eltahir, 1998). In a companion paper, Zheng and Eltahir (1998) employed a numerical model (of their own design) to determine the rainfall response to large-scale soil moisture anomalies focusing on processes related to the West African summer monsoon. The results of the numerical experiments were able to isolate the important contribution of radiative and dynamical feedback pathways influencing soil-moisture rainfall feedback (Zheng and Eltahir, 1998).

Many studies of land-atmosphere coupling have used climate models to conduct their analyses, however no climate model to date has ever proven to accurately replicate all aspects of the global climate. Therefore, when conducting analyses using climate models it is important to consider their limitations in replicating the natural world. In this vein, Lawrence et al., (2007) made a significant contribution toward understanding land-atmosphere coupling by investigating the partitioning of evapotranspiration in general circulation models (GCM) compared to observations. They classified three components of evapotranspiration—transpiration, soil evaporation and canopy evaporation. According to estimates from the Global Soil Wetness Project 2 (GSWP2), transpiration comprises the dominant component of total evapotranspiration (ET), followed by soil evaporation and canopy evaporation. By comparison, the National Center for Atmospheric Research (NCAR) Community Land Model version 3 (CLM3) (Bonan and Levis, 2006) selects soil moisture evaporation and canopy evaporation as the largest components followed by transpiration. Model experiments found that stronger transpiration and reduced canopy evaporation result

in an extended response to rain events by ET, and a shift in precipitation patterns toward more frequent, smaller events. The authors also noted that weaker contributions from transpiration in ET might affect the amplitude and regionality of land-atmosphere coupling in CLM3 and the NCAR Community Atmosphere Model version 3 (CAM3) (Hurrell et al., 2006) and stressed the importance of accurate ET partitioning when modeling the hydrologic cycle, especially as more complex hydrological schemes are introduced.

Conversely, Wu and Dickinson (2005) studied model (CAM3-CLM3) simulations of warm season (JJA) rainfall variability over the Great Plains compared with observations to determine the validity of land-atmosphere interactions in the model. Their results showed that for the Great Plains region, rainfall variability is connected to evapotranspiration anomalies but primarily the evaporation component rather than transpiration—which differ from the global results of Lawrence et al. (2007). The two studies did agree, however that the contribution from evaporation was much greater than transpiration and therefore the effects of soil moisture were likely to be underrepresented by the model. The difference between these two conclusions may indicate something unique about the regional climate of the Great Plains.

Dai et al., (1999) also investigated the accuracy of model-generated hydrologic cycles. Using observations and the NCAR regional climate model (RegCM) with three different cumulus convection schemes, they analyzed diurnal precipitation variations over the United States. The diurnal cycling of precipitation frequency and intensity plays a large role in surface hydrological process—for example rain that falls in the afternoon is more likely to be evaporated than rain that falls at night. They found that all three convection schemes had difficulty reproducing patterns of diurnal precipitation over the U.S., especially the NCAR

Community Climate Model version 3 (CCM3), the predecessor of CAM3, which rained too much over the Southeast due to overly frequent convection parameterizations. This is significant because climate models are frequently tuned to reproduce average precipitation accumulations but, as found in the study by Dai et al. (1999), models often are able to reproduce observed daily or monthly climatologies without accurately reproducing diurnal patterning of precipitation events. Additionally, overly frequent precipitation events may inflate land-atmosphere coupling calculated from models by exaggerating the frequency of the positive feedback mechanism.

Dirmeyer (2006) studied the hydrologic feedback pathway for land-atmosphere coupling by following the propagation of forced moisture anomalies using the Center for Ocean-Land-Atmosphere Studies (COLA) climate model. Results suggested soil wetness and latent heat flux anomalies were most persistent in dry regions due to the water holding capacity of the soil being large compared with the magnitude of water fluxes between atmosphere and land. The author speculated that predictability of precipitation from land-atmosphere coupling would be limited to certain locations and seasonalities—consistent with the findings of Wu and Dickinson (2005) in the Great Plains.

A pair of papers by Ruiz-Barradas and Nigam (2005, 2006) examined the contributions of remote and local moisture sources to North American precipitation variability as well as the importance of soil moisture in generating local, and large scale hydroclimate variability. The authors stress the importance of understanding regional climate processes before investigating climate change effects upon them. Comparisons between several sets of climate models and observations revealed that evaporation anomalies are perhaps too strong in model simulations. In the models, local moisture sources were

larger than remote sources while the opposite was found in observations, indicating that precipitation recycling within the models is overly efficient and therefore warm-season land-atmosphere coupling is likely to be over-emphasized in North America (Ruiz-Barradas and Nigam, 2005). In their follow-up analysis, the authors repeated their study using 6 IPCC climate models. Two of the models exaggerate local recycling of precipitation due to evapotranspiration, two models do just the opposite and place a premium on remote moisture sources while ignoring the influence of local land-surface process and the remaining two models appear to partition the moisture sources accurately (Ruiz-Barradas and Nigam, 2006). The accurate partitioning of soil moisture sources is therefore also an important consideration when calculating land-atmosphere coupling using models.

Wetherald and Manabe (2002) endeavored to study the change of land-surface hydrology associated with climate change using a coupled ocean-atmosphere-land surface model. Results showed that in Northern Hemisphere mid-latitudes, summer soil moisture decreases, while winter soil moisture increases—except in semi-arid regions where soil moisture is diminished during most of the year. These results are broadly consistent with Dirmeyer's (2006) assessment that land-atmosphere coupling appears to be most prominent in dry regions and therefore regions of interest concerning land-atmosphere amplification of climate conditions.

One of the most prolific contributors to the study of land-atmosphere coupling is Randal Koster (Koster et al., 2006; Mahanama and Koster, 2005; Koster and Suarez, 2004; Koster et al., 2004; Mahanama and Koster, 2003; Koster et al., 2003; Koster et al., 2002). His work has included extensive analysis of land-atmosphere coupling employing a swath of models with observational verifications where available. Koster et al. (2002) proposed a

more general mechanism for the positive soil moisture feedback than Eltahir (1998) using the concept that wetter soil induced higher evaporation leading to additional precipitation via local recycling as well as modifications in large scale circulation—identifying that strong soil moisture anomalies might be used for short term and seasonal precipitation predictions serving as a kind of "moisture memory" source for future precipitation. To test this theory, Koster et al. (2002) performed a controlled numerical experiment using four different atmospheric general circulation models (AGCMs) to compare the inter-model variability of land-atmosphere coupling exhibited by models, focusing on synoptic timescales. Results of the numerical analysis showed significant variation in land-atmosphere coupling between models. The authors attributed these variations to uncertainty in model parameterizations of boundary conditions and convection (Koster et al., 2002). Successive studies further analyzed model capture of land-atmosphere processes by comparing results from AGCMs to observations (Koster and Suarez, 2004; Koster et al., 2003), conducting experiments on land-surface models to study model differences in soil moisture memory behavior (Mahanama and Koster, 2003) in addition to climate bias analysis of the evaporative sensitivity to soil moisture using different vegetation schemes (Mahanama and Koster, 2003). Significant results from these studies include: co-location of land-atmosphere coupling regions between models and observations indicating that land-atmosphere feedbacks either exist in nature or the AGCMs reproduce the patterns for the wrong reasons (Koster and Suarez, 2004; Koster et al., 2003); soil moisture memory is highly dependent on hydrological parameterizations in the models, particularly the sensitivity of evaporation to soil moisture (Mahanama and Koster, 2003); and land-surface schemes in models do not always behave as they should in that they were found to inaccurately shift surface evaporative regimes between atmosphere

controlled states (wet climates) and soil moisture controlled states (dry climates) and vice versa (Mahanama and Koster, 2005).

Certainly the most widely known contributions by Koster to the study of land-atmosphere coupling are from the Global Land-Atmosphere Coupling Experiment (GLACE) that produced the Koster et al. (2004) "Hot Spot" paper. GLACE was an extensive inter-model comparison project that used 12 different AGCM modeling groups to perform the same highly controlled numerical experiments—similar to Koster et al. (2002), but on a larger scale. Each model experiment used a 16-member ensemble simulation where soil moisture evolved freely in the model and another 16-member ensemble where soil moisture

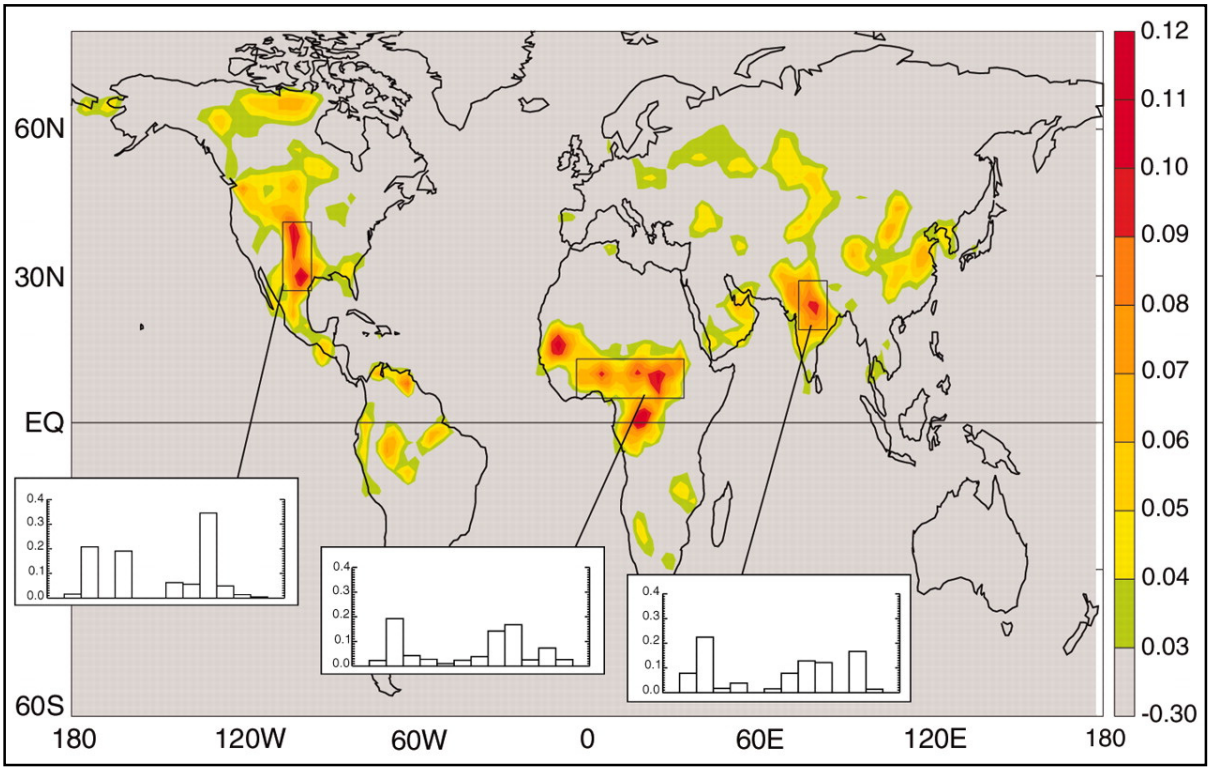

Fig 2.1. *Land-atmosphere coupling strength for boreal summer, describing the impact of soil moisture on precipitation averaged across 12 models from Koster et al., (2004) and the GLACE experiment. Insets are histograms of coupling strengths across the 12 models for each of the three "Hot Spots" outlined in boxes. Evident in the histograms is the large spread among model coupling strength such that results derived from model averages will be dominated by the strongest signals.*

was forced to be the same across all 16 ensembles (Koster et al., 2006). The difference between the two ensembles (denoted W and S, respectively) approximates the fraction of precipitation variance explained *only* by the variance in soil moisture. The same method was also applied to temperature and soil moisture, not discussed here. Figure 2.1 shows the Hot Spot map from Koster et al., (2004) calculated from this land-atmosphere coupling metric, averaged across all 12 models. Co-located Hot Spots for land-atmosphere coupling occur in the North American Great Plains, the African Sahel (see Fig. 2.3), and northern India. The highest land-atmosphere coupling strengths show soil moisture accounts for approximately 20% of synoptic scale precipitation variability (Koster et al., 2006). The authors note that these Hot Spots occur in transition-zones between humid and dry climates—semi-arid regions where "the atmosphere is amenable to precipitation generation [in particular, where

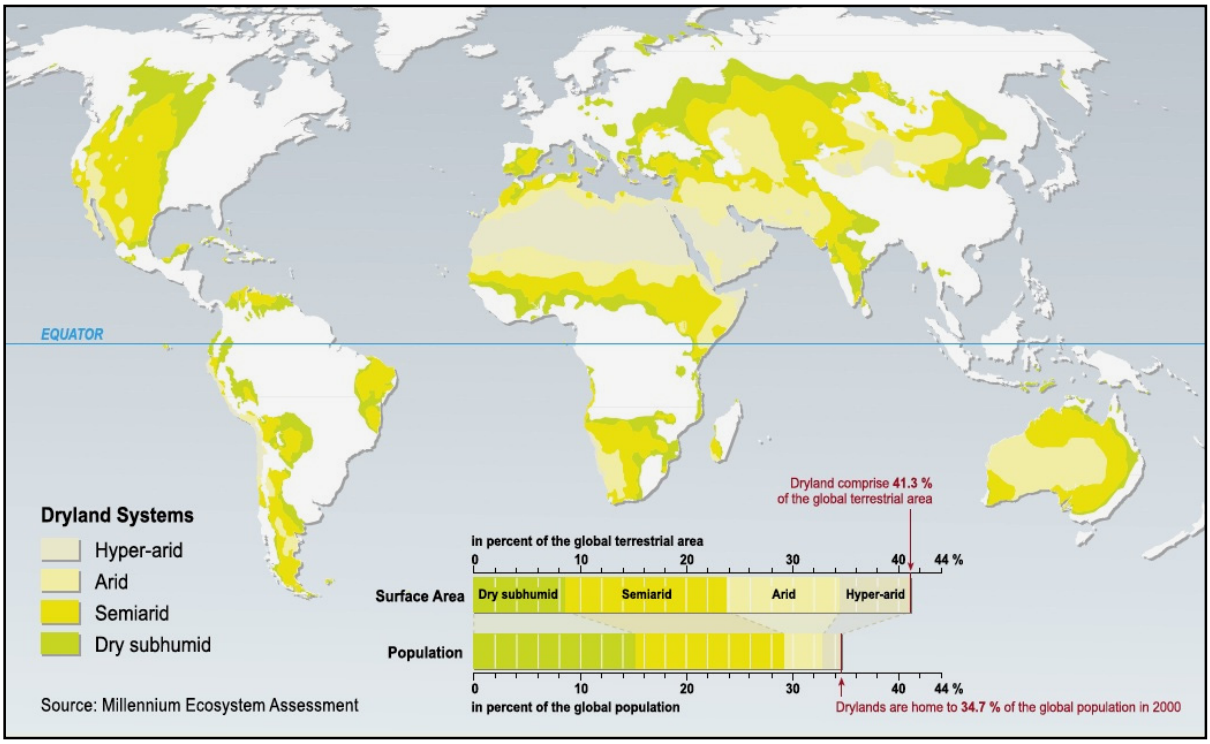

Fig. 2.2. *Global distribution and classification of arid land.*

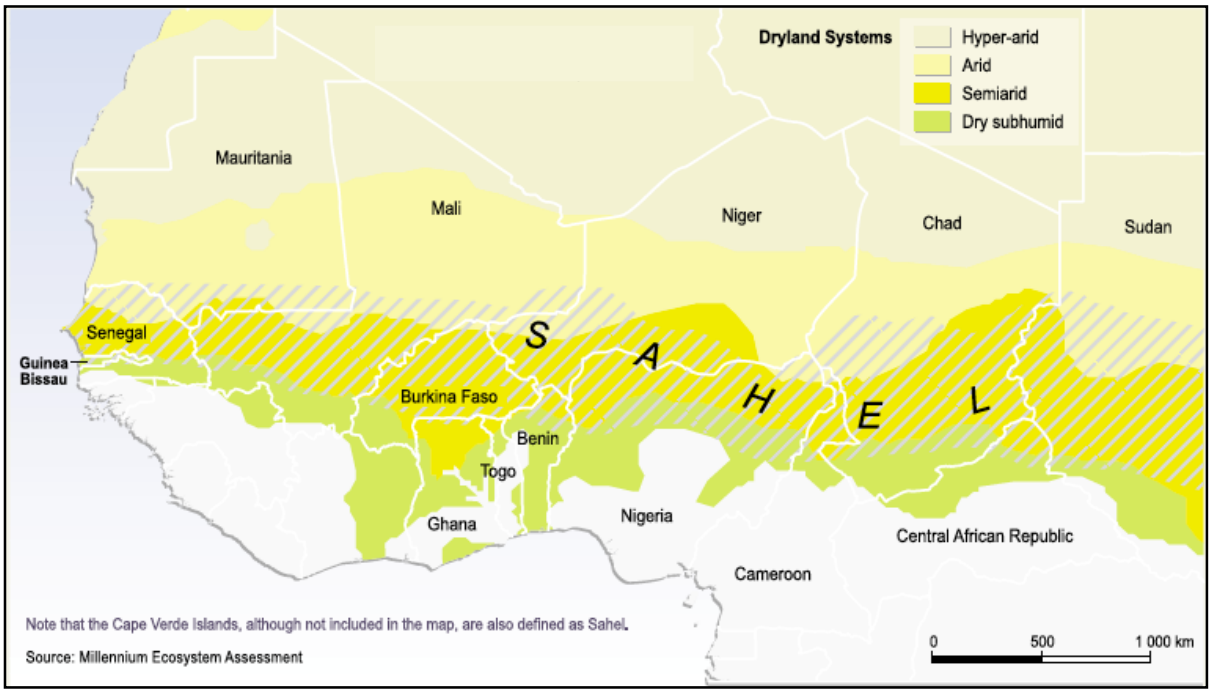

Fig. 2.3. *The Sahel region of Africa lies on the southern border, or "shore" of the Sahara desert and is primarily a semi-arid region that has been devastated since the 1970's by successive years of drought and famine with little recovery (Biasutti and Giannini, 2006; Foley et al., 2003).*

boundary layer moisture can trigger moist convection] and where evaporation is suitably high, but still sensitive to soil moisture" (Koster et al., 2004). For comparative purposes, a map of global arid land is shown in Figure 2.2 and the location and climatology of the African Sahel is shown in Figure 2.3.

Embedded histograms illustrate the model spread for each boxed Hot Spot. Models with large coupling strength have atmospheres very sensitive to evaporation variations, whereas models with low coupling strength have atmospheres relatively insensitive to evaporation (Guo et al., 2006). Ruiz-Barradas and Nigam (2006) were skeptical of the GLACE results because model averages are easily influenced by a few models with the largest signals—especially evident in the models over North America—however, while the GLACE authors concede that magnitudes of land-atmosphere coupling are largely influenced

by a few strong models, they maintain that the co-location of regions of strong land-atmosphere coupling (relative to each model) is not insignificant (Koster et al., 2004). The authors put forth these Hot Spots as land analogs to the ocean's El Nino Hot Spot in the Eastern Tropical Pacific, which can be used to predict ocean temperature anomalies more than a year in advance (Koster et al., 2004). A final note on the GLACE study is that their method for assessing land-atmosphere coupling strength did not distinguish between local and remote land surface influence on precipitation (Guo et al., 2006). While it is unclear whether local versus remote moisture sources have a greater impact on land-atmosphere feedbacks in nature, the work by Ruiz-Barradas and Nigam (2005, 2006) discussed earlier introduces another level of model variability in that models that have an over-emphasis on local precipitation recycling might exhibit strong land-atmosphere coupling and visa versa.

Shortly after the GLACE project result was published, many other studies assessing land-atmosphere coupling emerged. Several of these additional studies examine land-atmosphere coupling in Europe—a region not considered a Hot Spot by the GLACE study (Giorgi et al., 2006; Seneviratne et al., 2006), while other studies employ a global approach but use different methods for assessing land-atmosphere coupling strength (Zhang et al., 2008; Notaro et al., 2008).

Seneviratne et al., (2006) used a regional climate model (RCM), in addition to IPCC AR4 models from the 20th century (20C3m) and Special Report on Emissions Scenarios A2 (SRES A2) model runs to investigate the feedback mechanisms responsible for predicted summer temperature variability in Europe that were not identified by the GLACE study. The authors employed three different methods to assess land-atmosphere coupling; variance analysis of JJA mean summer temperature, GLACE-type coupling strength parameter (with

some differences), and a correlation between JJA temperatures and evapotranspiration. Their results reported an increase in climate variability resulting from land-atmosphere interactions associated with climate change induced northward shifting climate regimes creating a new transition zone in central and eastern Europe with strong land-atmosphere coupling (Seneviratne, 2006). Although GLACE did not include Europe as a Hot Spot region, these results imply that in the future, parts of European climate will become semi-arid and a region of strong land-atmosphere coupling.

2.2 LAND-ATMOSPHERE COUPLING: A STATISTICAL APPROACH

Instead of conducting model experiments, Giorgi (2006) developed a Regional

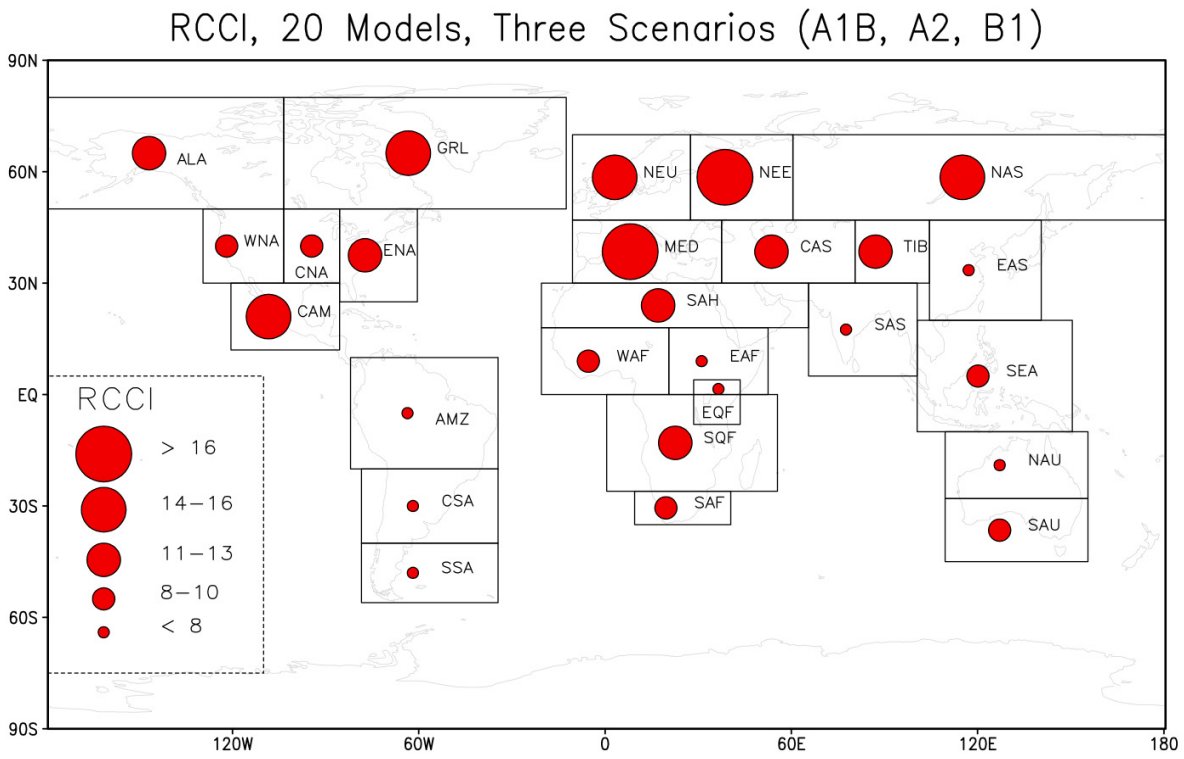

Fig. 2.4. *Quantifying land-atmosphere coupling through a regional climate change index (RCCI) calculated with climate models across three future emissions scenarios from Giorgi (2006).*

Climate Change Index (RCCI), using regional mean precipitation changes, mean surface air temperature changes, and changes in interannual precipitation and temperature variability. Giorgi (2006) generated his RCCI for 20 IPCC models using three different future emissions scenarios (SRES A1B, A2, B1) compared to the 20th century. The RCCI was designed to identify regions of the globe that will be most responsive to climate change—Giorgi's definition of a "Hot Spot." A map of these multi-model scenario-averaged Hot Spots is shown in Figure 2.4, notice that two of the most prominent Hot spots are found in northeastern Europe and the Mediterranean—consistent with Seniveratne et al.'s (2006) model experiment forecast that Europe would become a region of strong land-atmosphere coupling in the future, yet also not directly comparable to the GLACE study because it relies on mean changes and interannual variability between present day and future projections.

Notaro (2008) did, however, conduct a global analysis to identify Hot Spots that are comparable to the GLACE study. Using monthly precipitation and soil moisture data from 19 IPCC AR4 models of the pre-industrial control (PICNTRL) Notaro employed a statistical method of lagged covariance ratios to quantify soil moisture-atmosphere feedback such that the lagged covariance of soil moisture and precipitation was divided by the lagged autocovariance of soil moisture. Figure 2.5 shows a map of mean JJA 1-month lagged soil moisture feedback across all 19 models. The locations of Hot Spots using the soil feedback method broadly agree with those of GLACE, suggesting that the Hot Spots are robust among models, even though their magnitudes are small (Notaro, 2008).

A consistent deficiency among many of the studies discussed in this section is the lack of suitable observations with which to compare model simulations. While observations do exist, it is difficult to find data sets of sufficient spatial and temporal scale to reliably

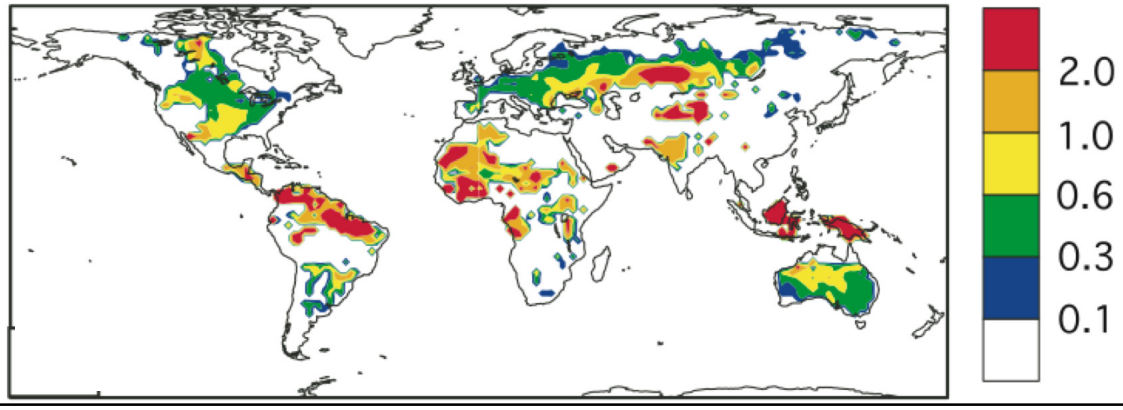

Fig. 2.5. *Quantifying land-atmosphere coupling through a soil moisture feedback parameter calculated with climate models for JJA from Notaro (2008). Statistic estimates the impact of total soil water on precipitation in units of (cm/month)/(40 kg/m^2) where 40 kg/m^2 represents a typical standard deviation in total soil water over the central U.S. feedback hotspot (Notaro, 2008).*

conduct analyses. Adequate observations for soil moisture, even on a regional basis, are especially rare. Zhang et al. (2008) attempted to account for this deficiency in the literature by using available precipitation observations from the Climate Prediction Center (CPC) Merged Analysis of Precipitation (CMAP) data derived from rain gauge observations, satellite estimates and National Centers for Environmental Protection-National Center for Atmospheric Research (NCEP-NCAR) reanalysis, and soil moisture data from the Global Land Data Assimilation System (GLDAS) generated by forcing three different land-surface models with ground and space-based observations.

The method for quantifying land-atmosphere coupling was the same used by Notaro (2008) as well as a variance analysis. Figure 2.6 shows the mapped results of both analyses, averaged across all three land-surface models used. Locations of Hot Spots calculated by Zheng et al. (2008) are not consistent with those from GLACE, but are somewhat consistent with those from Notaro (2008) –regions of large land-atmosphere coupling from this study broadly overlap with regions of little soil moisture feedback in Notaro (2008). It is curious,

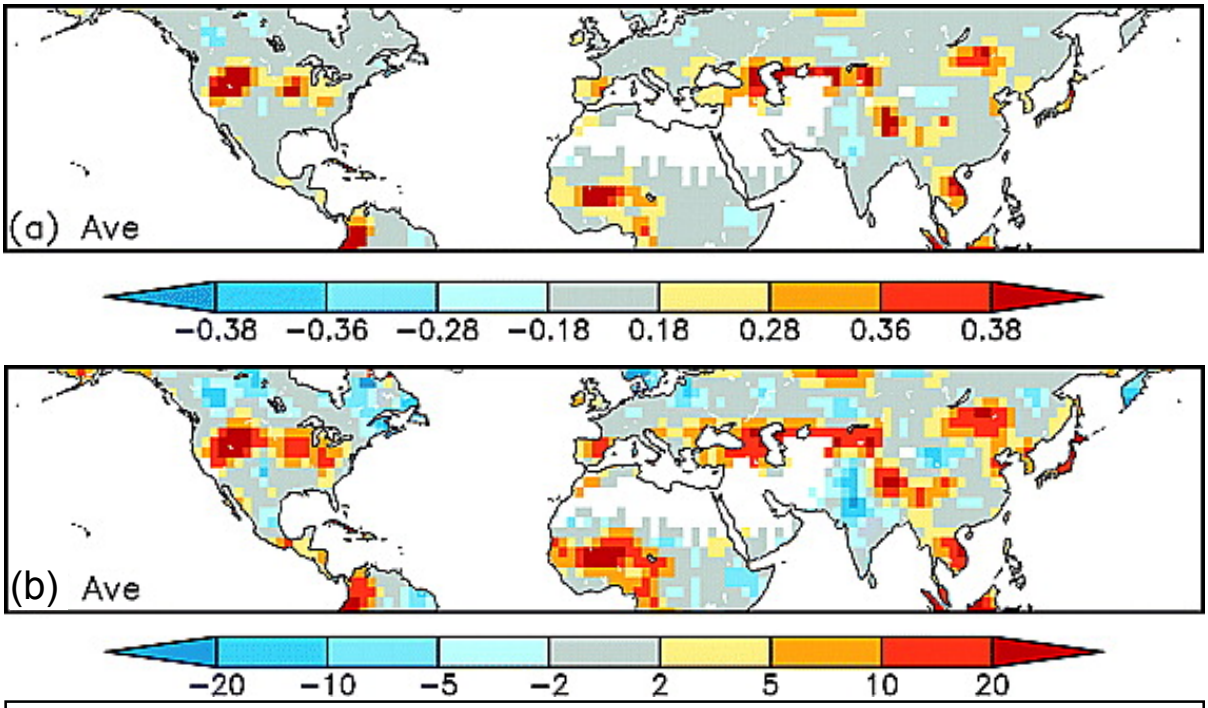

Fig. 2.6. *Quantifying land-atmosphere coupling through (a) correlations of monthly soil moisture anomalies leading CMAP precipitation anomalies by 1 month calculated using MJJ soil moisture and JJA precipitation and averaged across three land-surface models and (b) the percentage of variance of monthly precipitation anomalies due to soil moisture feedback calculated using JJA soil moisture and precipitation averaged across three land-surface models. Figures from Zhang et al., 2008.*

however, that regions of strong land-atmosphere coupling common to several studies described in this section, such as the North American Great Plains, were not identified in this study. The authors attribute differences in timescales—seasonal versus synoptic for the incompatibility between their method and the GLACE study (Zheng et al., 2008). However, given the results of Notaro (2008), which match both the GLACE and Zheng et al. (2008) results to some degree, the differences are more likely associated with the use of observations as opposed to models. This finding highlights the importance of comparison between models and observations and the relative ease of doing so when a statistical method is used to calculate land-atmosphere coupling because statistical methods may be easily performed on both—which is not true of highly controlled numerical experiments. It also highlights the

need for genuine observational data, particularly for global soil moisture, as the data used in this study was derived from data assimilated models.

This review presented a sampling of the two prominent methods for quantifying land-atmosphere coupling in the scientific literature, model experiments and statistical tests. The method employed by this study to quantify land-atmosphere coupling is similar to the statistical method presented in Notaro (2008) and Zheng et al. (2008), uses both model products and observations, and will be compared to the model experiment results of Koster et al. (2004).

CHAPTER THREE: LAND-ATMOSPHERE COUPLING

3.1 THEORY

This research employs a statistical lagged correlation method to quantify global regions of land-atmosphere coupling. The method is derived from one used by Frankignoul et al. (1998) to investigate interactions between sea surface temperatures (SSTs) and the atmosphere, and used by Liu et al. (2006) for vegetation-climate interactions. The purpose of the correlation method is to determine the existence of a positive feedback loop within the hydrologic cycle. This study hypothesizes that a positive hydrologic feedback exists such that precipitation increases soil moisture, and soil moisture is evaporated into atmospheric moisture available for more precipitation. Using lagged correlation presumes that feedbacks are not instantaneous and instead evolve over some synoptic timescale, introducing a repository of transferable moisture memory into the hydrologic cycle.

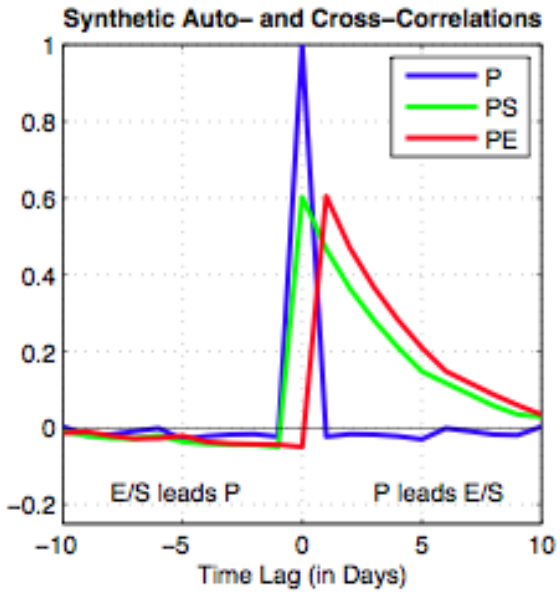

Fig. 3.1. *Auto-correlation of P and cross-correlations of PS and PE generated from synthetic data. Precipitation series is generated with random numbers from 0-1 for 50 years of 100-day "summers". Evaporation series is equivalent to the soil moisture series multiplied by a dampening term (α=1/5). Soil moisture series was generated by equation (2).*

First, however, let us consider the null hypothesis; a simplified version of the hydrologic cycle that has no precipitation memory and soil moisture that only changes with atmospheric inputs and outputs (i.e. there is no runoff, or percolation).

$$\frac{dS}{dt} = (P - E) \quad (1)$$

Where P is precipitation, S is soil moisture and E is evaporation. Choosing a time step of dt=1 for simplicity, the equation may be re-written:

$$S_i = S_{i-1} + (P_i - E_i) \quad (2)$$

Further assume, that evaporation is only limited by the availability of soil moisture and not by energy input such that the only sink for soil moisture is through evaporation at the soil surface (see section 3.2 for a more complete explanation of this):

$$E = \alpha * S \quad (3)$$

Where α is a dampening term, then

$$(S_i - S_{i-1}) = P_i - \alpha * S_{i-1} \quad (4)$$

Based on these hydrological simplifications, soil moisture may be approximated as an auto-regressive type 1 (AR1) process with a large memory forced by the atmosphere. If precipitation is taken to behave as white noise (N_a), then we can expect its lagged autocorrelation will exhibit no memory and be zero everywhere except at lag-zero where it will be one. Cross-correlating precipitation with soil moisture demonstrates the effect of current precipitation on later soil moisture, as well as the effect of current soil moisture on later precipitation via evaporation. These relationships define the positive feedback loop where precipitation increases soil moisture, which increases evaporation, which increases atmospheric moisture available for later precipitation. In Figure 3.1, correlations have been performed using synthetic data generated from the simple hydrological model outlined in this section. The shorthand-labeling scheme used in the figure legend and throughout this text denotes PE for the lagged cross-correlation of precipitation and evaporation, PS for the

lagged cross-correlation of precipitation and soil moisture, and simply P for the autocorrelation of precipitation. For positive lags, precipitation is leading soil moisture and as one would expect; soil moisture and precipitation are highly correlated because after it rains, the soil is wetter. Evaporation and precipitation are similarly correlated because wetter soil promotes evaporation—and we have assumed evaporation is dependent on soil moisture. For negative lags, correlations are essentially zero, implying that soil moisture behaves like an AR1 process and increases only through the noise forcing of precipitation, which exhibits no feedback with evaporation or soil moisture because there is no mechanism through which evaporation can influence later precipitation—the null hypothesis for this analysis.

Studies of soil and precipitation variability on monthly to seasonal scales contradict this null hypothesis and assert the existence of land-atmosphere feedback (see Chapter 2). Despite the prolificacy of land-atmosphere coupling studies in the literature, there is no single, universally accepted definition of what determines land-atmosphere coupling or how best to quantify it. This study examines hydrologic feedbacks on synoptic timescales, therefore the slow variability of the soil moisture column resulting from its large moisture memory make it unsuitable for lagged correlation analysis on shorter, synoptic timescales. Following from Ruiz-Barradas and Nigam (2006), moisture that falls to the surface as precipitation can be partitioned into local moisture sources from evaporation, and remote moisture sources through convergence of large-scale atmospheric moisture transport. To the extent that local evaporation represents the dominant source of moisture for precipitation, one would expect that precipitation is sensitive to previous evaporation and therefore local soil moisture. In a region where this is the case, one could imagine that hydrological extremes may become self-perpetuating since a lack of precipitation would lead to reductions

in soil moisture followed by reduced evaporation leading to further reductions in precipitation. For the purposes of this study, land-atmosphere coupling will be defined by the lagged cross-correlation of precipitation with evaporation. Using this cross-correlation method, land-atmosphere feedbacks are expected to manifest in the positive correlation of evaporation leading precipitation. This statistical method is extremely useful because it may be easily applied to products of GCMs and observational data alike, without the need for complex model experiments.

3.2 METHODS

Data: Models and Observations

For this analysis, daily precipitation (pr) and latent heat flux (hfls) data from available IPCC AR4 "Climate of the 20th Century Experiment (20C3M)" (PCMDI, 2007; IPCC, 2007c) models were used (see Table 3.1). These models were part of the Coupled Model Intercomparison Project phase 3 (CMIP3) (Meehl et al., 2007) and cover 40 years best comparable to 1961-2000, except CCSM3.0, which includes 50 years comparable to 1950-1999 (PCMDI, 2007). Two models available in the CMIP3 data set but not included in this study are FGOALS and GISS-ER, which were eliminated after preliminary analysis due to an inability to reproduce broad climatic features indicating the model does not represent the state of the science (Zhang and Walsh, 2006) and magnitude errors in precipitation data suggesting data file corruption, respectively.

Observational data of high spatial resolution and long temporal period are not currently available on a global scale. There are, however, such data for North America from the National Centers for Environmental Protection's (NCEP) North American Regional

Reanalysis (NARR) (Mesinger et al., 2006). NARR is a relatively long-term (1979-present), high-resolution atmosphere and land surface hydrology dataset that assimilates precipitation and is successful at reproducing climatological patterns, capturing diurnal cycles and regional hydrological cycles (Mesinger et al., 2006; Ruiz-Barradas and Nigam, 2006). NARR data used in this study includes daily precipitation, evaporation and soil moisture.

A dataset from the Variable Infiltration Capacity (VIC) model—a macroscale

	Group	Country	Model ID
1	Bjerknes Centre for Climate Research	Norway	bccr_bcm2_0 (BMC2)
2	Canadian Centre for Climate Modelling & Analysis	Canada	cccma_cgcm3_1 (t47) (CGCM3)
3	Canadian Centre for Climate Modelling & Analysis	Canada	cccma_cgcm3_1_t63 (CGCM3t63)
4	Météo-France / Centre National de Recherches Météorologiques	France	cnrm_cm3 (CNRM)
5	CSIRO Atmospheric Research	Australia	csiro_mk3_0 (CSIRO)
6	US Dept. of Commerce / NOAA / Geophysical Fluid Dynamics Laboratory	USA	gfdl_cm2_0 (GFDL)
7	NASA / Goddard Institute for Space Studies	USA	giss_aom (GISS)
8	Institute for Numerical Mathematics	Russia	inmcm3_0 (INMCM)
9	Institut Pierre Simon Laplace	France	ipsl_cm4 (IPSL)
10	Center for Climate System Research / National Institute for Environmental Studies / Frontier Researc Center for Global Change	Japan	miroc3_2_hires (MIROCh)
11	Center for Climate System Research / National Institute for Environmental Studies / Frontier Researc Center for Global Change	Japan	miroc3_2_medres (MIROCm)
12	Meterological Institute of the University of Bonn / Meterological Research Institute of KMA / Model and Data Group	Germany / Korea	miub_echo_g (ECHO)
13	Max Planck Institute for Meteorology	Germany	mpi_echam5 (ECHAM5)
14	Meterological Research Institute	Japan	mri_cgcm2_3_2a (MRI)
15	National Center for Atmospheric Research	USA	ncar_ccsm3_0 (CCSM3)

Table 3.1. *IPCC AR4 models from the 20C3M control experiment used in this study. Available models that were left out of the study include; the GISS-ER, left out due to data corruption in a portion of precipitation data and FGOALS which was not representative of the state of the science in climate modeling. In parenthesis next to models names are how the models are identified in the text.*

hydrologic model that spans the U.S. and parts of Canada and Mexico, and includes nearly 50 years of high-resolution precipitation, evaporation and soil moisture data—is also used as an "observation" dataset (Maurer et al., 2002). The VIC model incorporates surface forcings from observed precipitation, yet output differs from reanalysis products like NARR because both water and energy budgets at the land surface balance at every time step during the model run (Maurer et al., 2002).

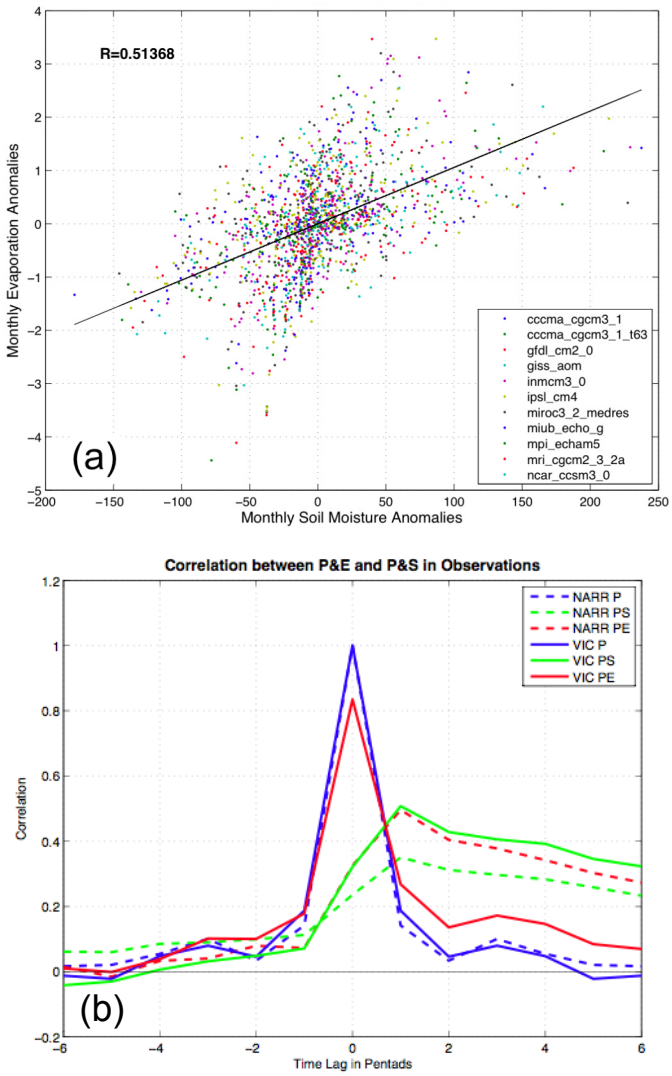

Fig. 3.2. *(a) Scatter of summer monthly evaporation (hfls) against soil moisture (mrso) for 12 IPCC models. Soil moisture accounts for about half the variance of evaporation in the monthly products. (b) Auto- and cross-correlations of summer observations in the Great Plains. Dashed lines are from NARR and solid lines are from VIC_NA. For both datasets, cross-correlations between P and E, and P and S exhibit similar negative lag correlation values.*

Although evaporation responds to both local soil moisture and remotely transported moisture sources, our simple hydrologic model in section 3.1 approximated evaporation as varying linearly with soil moisture. Figure 3.2a tests, and affirms that approximation by scattering model produced monthly JJA evaporation anomalies against soil moisture anomalies for a portion of the southern Great Plains in North America (32N-38N, 98W-104W). The

response of precipitation to both soil moisture and evaporation is also shown in Figure 3.2b where the lagged auto- and cross-correlations of precipitation with soil moisture (PS) and evaporation (PE) for both the NARR and VIC data over the same region of the Great Plains. In NARR, the cross-correlation patterns of PS and PE are fairly consistent. VIC by comparison appears to impart much more precipitation variability upon evaporation for positive time lags, however, negative lags are the focus of this study and both models consistently exhibit small correlation values there.

The VIC model has primarily, and successfully, been used to model large-scale river basins (Nijssen et al., 2001). Global data from the VIC model is also available, however at a lower spatial and temporal scale (1980-1993) (Nijssen et al., 2001; Nijssen et al., 1997), and is therefore used in a limited capacity for model comparison by this study. To distinguish between North American and global VIC data in figures and text from this point forward, they are referred to as VIC_NA and VIC_GLOB, respectively. Although data derived from the VIC models are technically model products, because they are forced with precipitation observations the collective set of NARR, VIC_NA, and VIC_GLOB will be referred to as "observations" throughout this paper.

Analysis

The following describes in detail all manipulations and calculations performed on the data. Except where noted, the same methods were applied to both GCM data and observations. Anomalies of precipitation and evaporation are extracted by first averaging daily data into five-day means (pentads), calculating, and removing (by subtraction) the annual cycle. The annual cycle is a climatology (averaged over all years) generated from

data smoothed using a five-pentad running mean. Pentad data is used rather than daily data, because it improves the signal to noise ratio (Lorenz and Hartmann, 2006).

Both precipitation and evaporation anomalies are then re-gridded by interpolation to a 2°x2° map grid (not performed on NARR and VIC_NA because the data used here have a 1°x1° resolution) before being spatially smoothed over a 6°x6° area. The smoothing method simply averaged each grid box equally with the 8 grid boxes adjacent to it, with no weighting. The anomalies were spatially smoothed because if data were analyzed without smoothing, the impact of soil moisture on precipitation 300km away would not be included in the land-atmosphere feedback of the correlation calculation—even though it still constitutes feedback (Koster et al., 2003). Using 6°x6° smoothing creates grid box areas that are approximately 665km x 580km near the tropics and 665km x 660km near the mid-latitudes.

Lagged correlations were calculated for the summer season (JJA=19 pentads) from the smoothed anomalies. Correlations were calculated by first calculating auto- and cross-covariances for each summer, for each model, for 13 time lags (-6 pentads to +6 pentads). Correlations were then calculated by dividing the annually averaged covariances by the annually averaged variances.

Statistical significance for the correlations were determined using a two-tailed t-test with a 95% confidence interval. Because lagged correlation values are expected to be small, it was necessary to determine positive and negative thresholds of significance from zero for each time lag, for each model using the following method from Salas et al. (1980):

$$r_{\tau}(95\%) = \frac{-1 \pm 1.96\sqrt{N - |\tau| - 1}}{N - |\tau|} \qquad (5)$$

Where τ is the time lag, 1.96 is the two-tailed t-value for a 95% confidence interval with more than 100 degrees of freedom, and N is the degrees of freedom, or sample size. The auto-correlation in the data indicates that the actual number of degrees of freedom is less than the number of data inputs; therefore, a method from Bretherton et al. (1999) must be employed to estimate the sample size for the significance test.

$$N^* = \frac{N}{\sum_{\tau=-6}^{6} \left[\left(1 - \frac{|\tau|}{N} \right) * \rho_\tau^P * \rho_\tau^E \right]} \qquad (6)$$

Where N* is the estimated sample size, N is the sample size of the originating data series (number of years * number of pentads), τ is again the time lag, and ρ_τ^P and ρ_τ^E are the lag τ autocorrelations of precipitation (P) and evaporation (E). The calculated value for N* was then substituted for N in (5) to calculate the positive and negative significance thresholds for lagged correlations. Results from these analyses are presented in the section that follows.

3.3 RESULTS AND DISCUSSION

Results from land-atmosphere coupling lagged correlation analysis are presented in Figures 3.3-6. IPCC model results for the same southern Great Plains region used in Figure 3.2b are shown in Figure 3.3, however the cross-correlations of precipitation and evaporation (PE) are presented in a separate figure from the autocorrelation of precipitation. Dashed horizontal lines on Figure 3.3a are the significance thresholds for a 95% confidence interval. Values greater than the positive bound, and less than the negative bound are significantly different from zero. The curious behavior of the ECHAM5 and ECHO models at lags 0 and +1 is a result that needs further study, however due to lack of statistical significance, they are

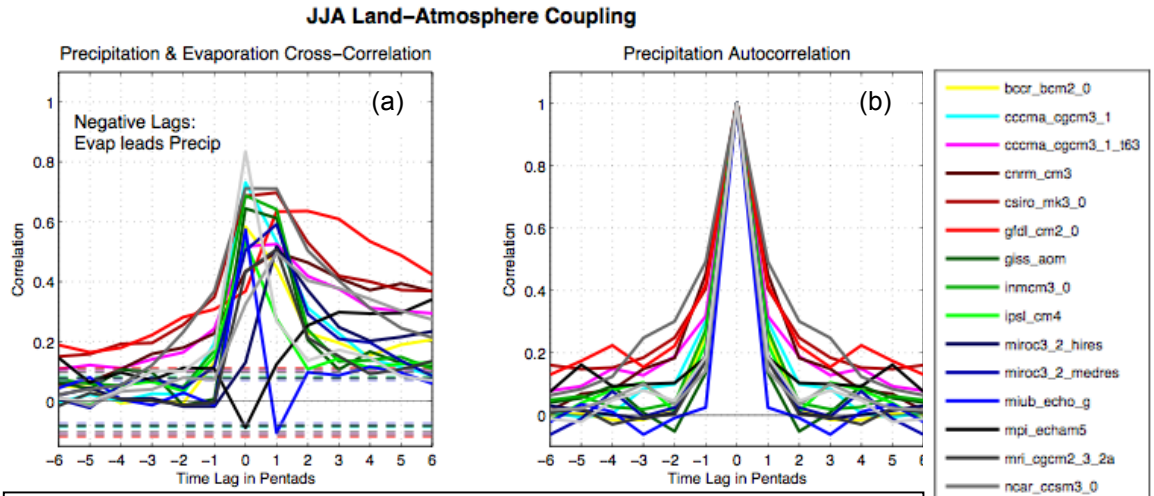

Fig. 3.3. *(a) Land-atmosphere coupling calculated used lagged correlation analysis for a region of the Great Plains (32N-38N, 98W-104W) with 15 IPCC models. Negative lags indicate that evaporation from the land surface is influencing later precipitation. (b) Lagged autocorrelation of precipitation exhibiting the spread in precipitation memory among models.*

not addressed here. Consistent with the results of many other analyses of land-atmosphere coupling, there is a significant spread among models. Notice, that the three models with largest correlations at lag -2 pentads (GFDL, CSIRO, CCSM3), are also the three models of highest value in the -2 pentad lag autocorrelation of precipitation. This result appears to satisfy the proposed theory that models with comparatively large land-atmosphere coupling, will also exhibit large precipitation memory. The relationship between precipitation memory and land-atmosphere coupling, at the longer timescale of 3 pentads (15 days) is shown in Figure 3.4. Here, the autocorrelation of P at the -3 pentad lag is plotted against the cross-correlation of PE at the -3 pentad lag for the same region of the Great Plains for all IPCC models and the NARR and VIC_NA observations. The visual assessment from Figure 3.2 is confirmed—precipitation memory is greater with larger values of land-atmosphere coupling strength.

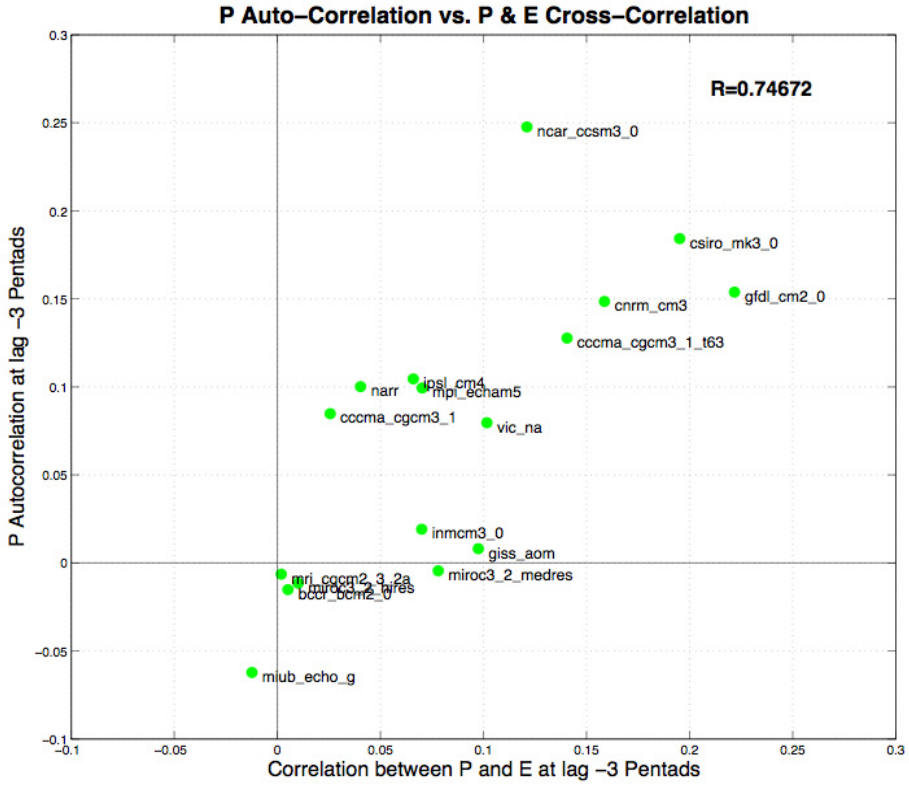

Fig. 3.4. *Autocorrelation of P at lag -3 pentads plotted against cross-correlation of PE at lag -3 pentads for 15 IPCC models and for NARR and VIC_NA. Again data is shown for the southern Great Plains region (32N-38N, 98W-104W). The models with large land-atmosphere coupling also exhibit large precipitation memory. Strongest models are CCSM3, CSIRO and GFDL.*

To this point results have focused on the southern Great Plains for the sake of model-observation comparability, however this is not the only region of the world where land-atmosphere coupling is strong. The IPCC model averaged PE correlation at -2 pentad lag is shown in Figure 3.5. For the remainder of this analysis, land-atmosphere coupling will be re-defined as the lag -2 cross-correlation of precipitation and evaporation because correlations between adjacent pentads are likely to be overly influenced by storms that straddle them (Koster et al., 2003), and 10 days is a sufficient time delay with which to investigate synoptic-scale land-atmosphere feedbacks. The map in Figure 3.5 includes 6°x6° boxes approximately positioned to match the strongest Hot Spots from Koster et al. (2004) located in the southern Great Plains of North America (32N-38N, 104W-98W), the Sahel in Africa (10N-16N, 18E-24E) and northern India (22N-28N, 72E-78E). The histograms below the

map match the boxes, and contain the correlation values for each model in that box (yellow bars are statistically significant from zero), numbers along the x-axis match the model numbers listed in Table 3.1.

In comparing Figure 3.5 with the GLACE Hot Spot map in Figure 2.1, it is immediately apparent that the regions of strongest land-atmosphere coupling do not manifest in the same locations, or with the same relative strength. As was previously mentioned,

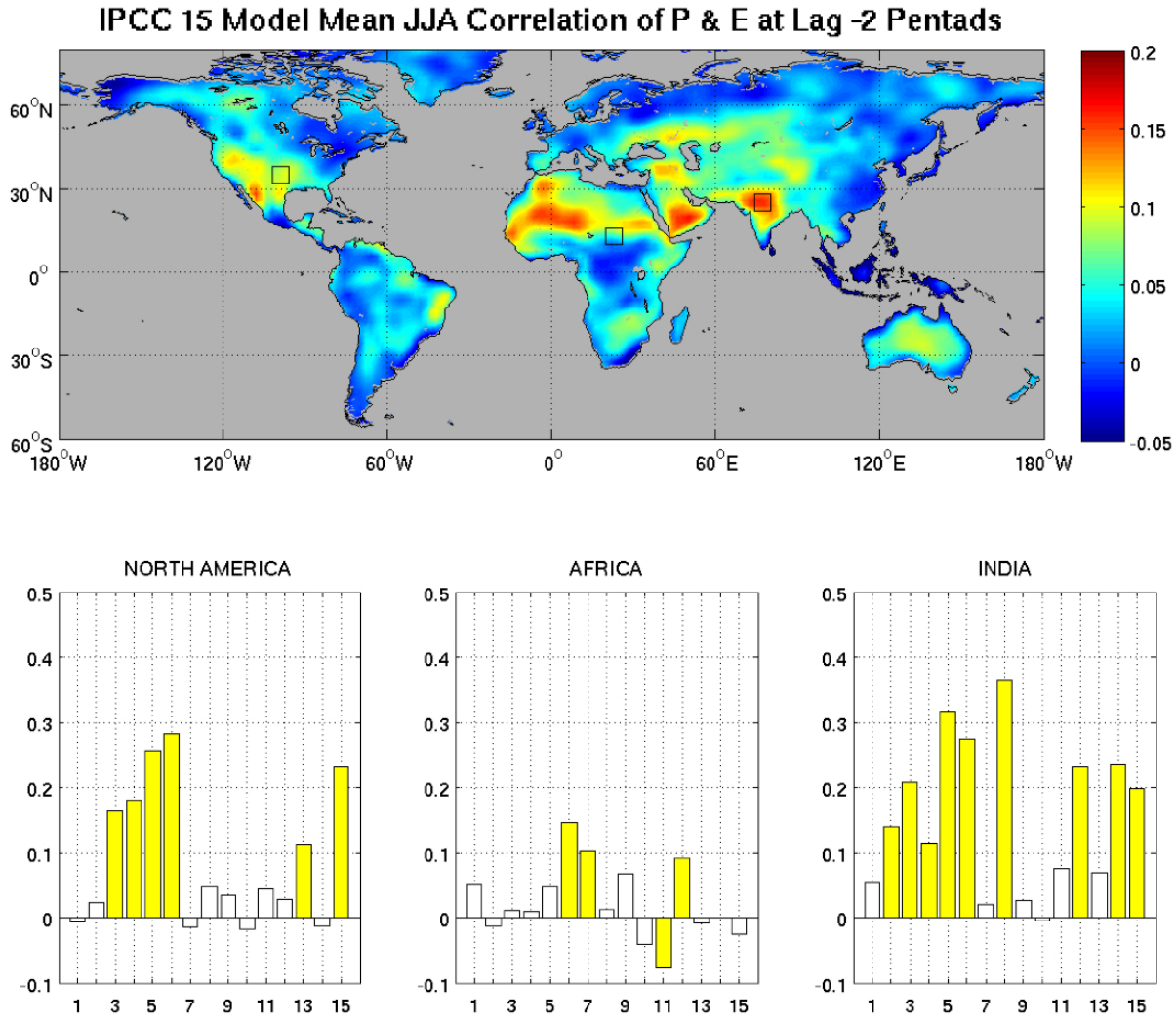

Fig. 3.5. *Model averaged global summer (JJA) land-atmosphere coupling measured as the lagged correlation of PE at -2 pentads where evaporation leads precipitation. Histograms show the coupling values for each model from three "Hot Spot" boxes in southern Great Plains, Sahel and northern India. Yellow bars are significant at the 95% confidence interval; numbers along the x-axis correspond to model numbers in Table 3.1.*

Ruiz-Barradas and Nigam (2006) criticized the results of the GLACE experiment because Hot Spot coupling strength appeared to be overly influenced by a few strong models. The same criticism may be made for the results of this study. Evident from the histograms in Figure 3.5 is the dominance of a few strong models. In the southern Great Plains, six models have correlations significantly different from zero, and of those, the CSIRO, GFDL and CCSM3 models have the largest values (> .20). In the Sahel, only four of the models have correlations significantly different from zero, most of those values are small, and one (MIROCm) is negative. Of the three Hot Spot boxes, India displays the most consistency among models; nine models have correlations significantly different from zero, and of those the CSIRO, GFDL, and INMCM have the largest values (>.25), with CGCM3t63, ECHO and MRI relatively large as well (>.20). Inter-model comparisons among this small global sample immediately identify the CSIRO and GFDL models as exhibiting large land-atmosphere coupling. For more extensive inter-model land-atmosphere coupling comparisons, Figure 3.6 shows the statistically significant (at 95% CI) global land-atmosphere coupling values for each model.

The MIROCh and ECHAM5 models exhibit generally weak or non-existent land-atmosphere coupling globally, as does MIROCm with the exception of a strong region over Saudi Arabia and the eastern Sahel. CNRM, CSIRO, GFDL, CCSM3 and to a somewhat lesser degree, CGCM3t63 all broadly agree on land-atmosphere coupling in the southern Great Plains while nearly two-thirds of the models agree on land-atmosphere coupling in northern India. The most contentious region regarding locations of global land-atmosphere coupling are found in northern and equatorial Africa. Several of the models exhibit very strong, perhaps unreasonably strong, land-atmosphere coupling across the Sahara desert and

Saudi Arabia—regions not identified as Hot Spots in the GLACE study. Large correlations in these desert areas may result from very small, yet highly correlated precipitation and

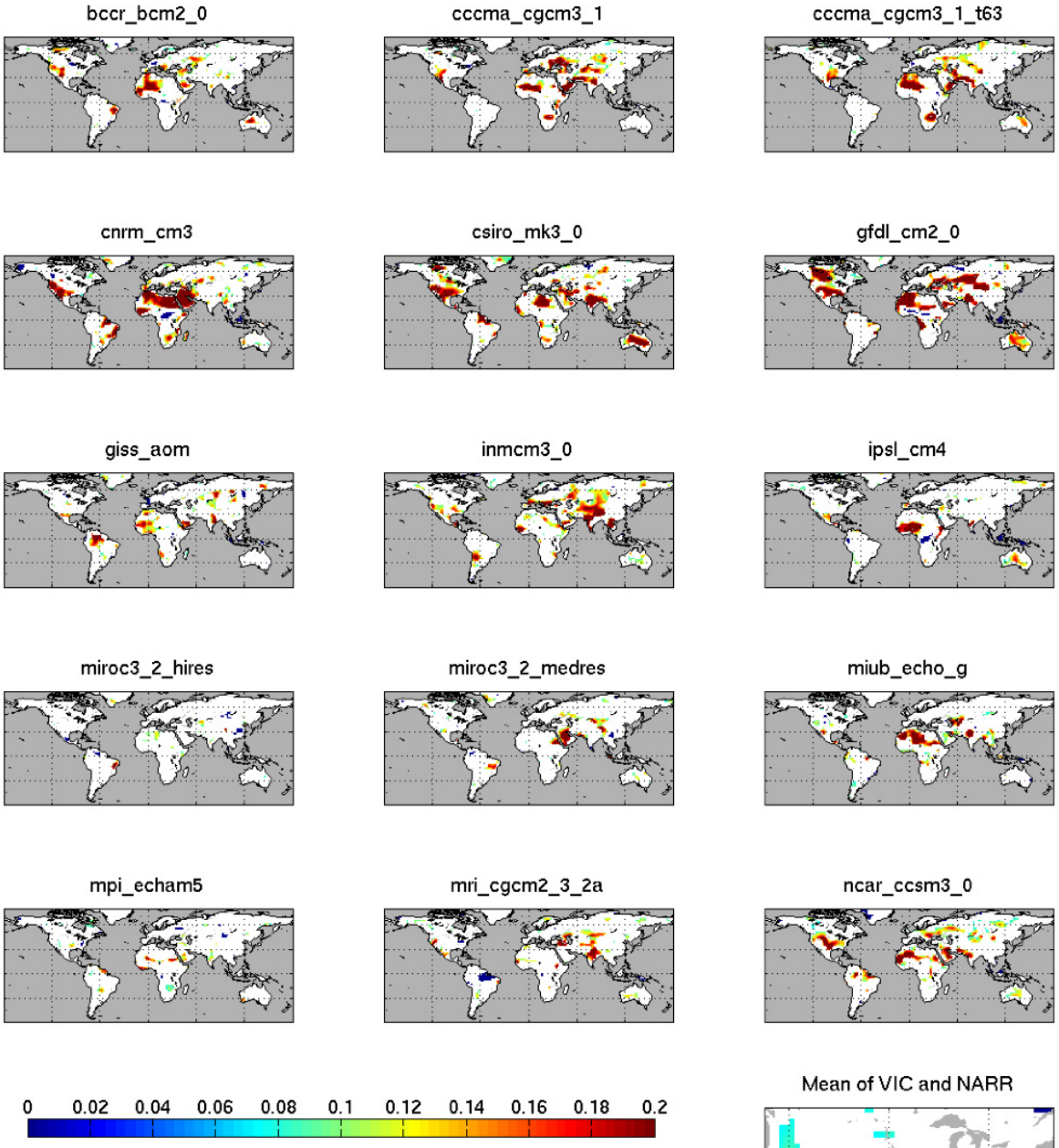

Fig. 3.6. *Statistically significant (at 95% CI) land-atmosphere coupling for 15 climate models as measured by the -2 pentad lagged correlation of PE (evaporation leads precipitation). Although adequate global observations were not available, the mean significant correlations for NARR and VIC over North America are included for comparative purposes.*

evaporation anomalies. Yet, because these regions are known to be hyper arid, it is expected that any moisture given to the soil from precipitation would be evaporated at time scales much shorter than two pentads. It is possible that in these desert regions, evaporation anomalies are induced by something other than soil moisture anomalies. For example, Hastenrath et al. (1993) found interannual precipitation variability in eastern Africa was closely connected to high phases of ENSO in the western equatorial Indian Ocean. Another

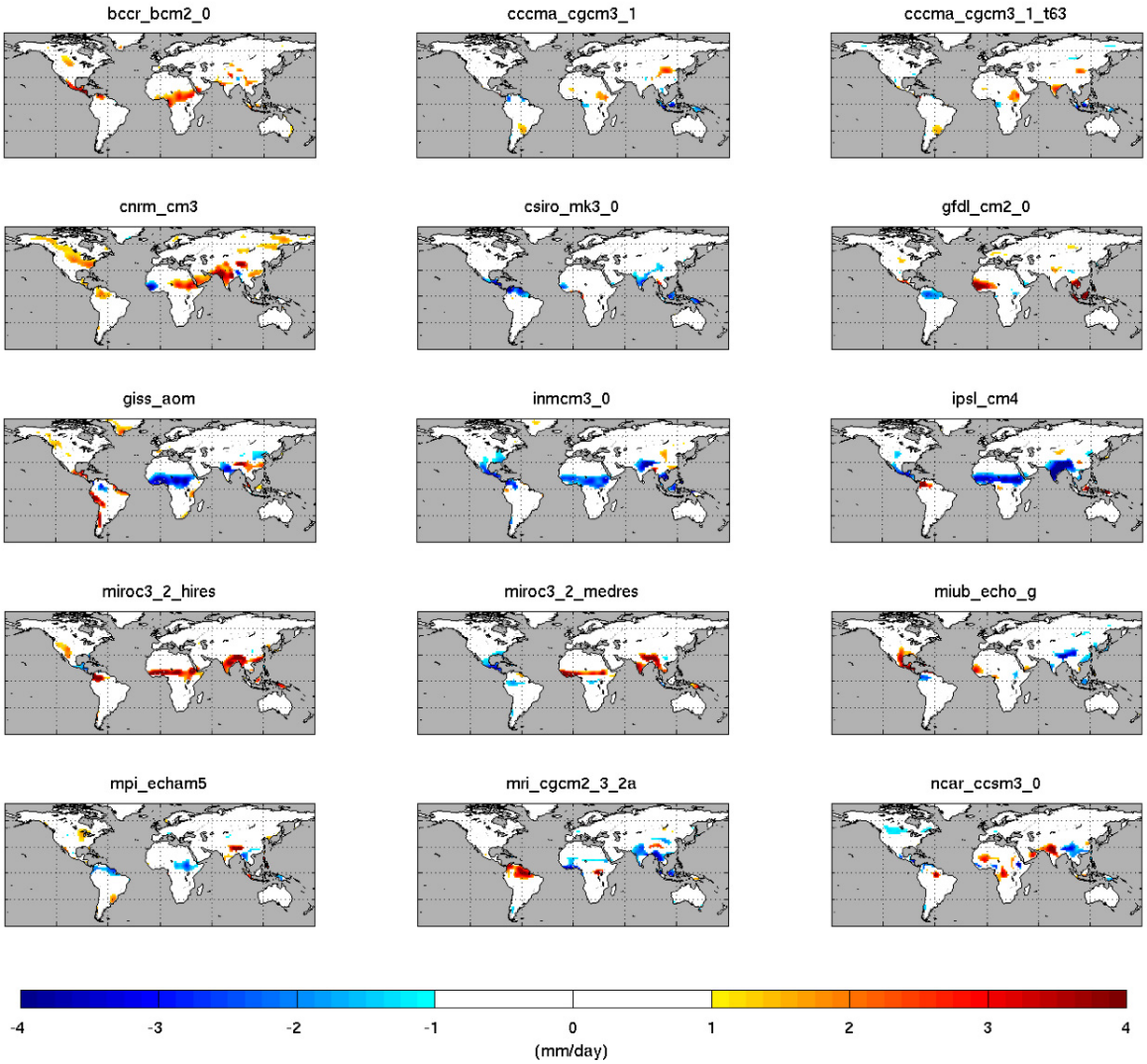

Fig. 3.7. *Model differences in summer precipitation from the 15-model mean. While models appear fairly uniform over the southern Great Plains—in contrast, precipitation patterns over Sahelian Africa, India and Saudi Arabia show substantial model disagreement.*

possibility is that models rain too much, or too frequently over these regions as Dai et al. (1999) found was the case in CCM3. Figure 3.7 shows model differences in summer (JJA) precipitation from the 15-model mean. Models are fairly consistent over the southern Great Plains, however, there appears to be a large amount of model disagreement over Sahelian Africa, India and in some cases Saudi Arabia. Large departures from the model mean may account for some of the unexpected Hot Spot regions.

When comparing the Hot Spot results of this study to that of the GLACE experiment, it is important to note that there is little overlap between the models used in GLACE and the IPCC models. Six models overlap the set, but of those only five are used here (but account for seven of the IPCC models because multiple versions of two models were used). The atmospheric components of CGCM3, CSIRO, GFDL, MIROC and CCSM3 were used in GLACE (data for the Hadley Center for Climate Prediction and Research / Met Office were unavailable). However, the differences in methods and models used between this and the GLACE experiment should indicate that co-located regions of strong land-atmosphere coupling in Figures 2.1 and 3.5 are in fact robust within the models. The primary finding of this analysis identifies co-located regions of land-atmosphere coupling appearing strongly in northern India, moderately in the Great Plains and to a lesser degree in the Sahel with strongest agreement in the western Sahel.

CHAPTER FOUR: 20th CENTURY DROUGHT

4.1 THEORY

Concepts of drought vary widely between climate regions (e.g. between tropical and arid climates) and this variety makes a single global definition for drought nearly impossible (Dracup et al., 1980). In addition, there are three universally recognized physically based forms of drought: meteorological, hydrological and agricultural. Meteorological drought is measured by a shortage of precipitation, hydrological drought is measured through a deficiency in the water supply relating to reservoir storage and streamflow, and agricultural drought is measured by a shortage in water available for plant growth—or sufficient soil moisture to replace evapotranspirative loss (Keyantash and Dracup, 2004). The best method for quantifying drought is highly dependent both on the type of physical drought examined as well as the particular drought characteristic of interest: drought severity, magnitude, frequency, persistence or spatial extent (McKee et al., 1993; Dracup et al., 1980).

If drought events are taken to behave as a stochastic process, then investigation of drought behavior on short time scales may be extrapolated out to longer time scales. In other words, the behavior of a model's depiction of drought in the future may be predicted from its behavior in the past. The focus of this analysis is on the persistence of drought events during boreal summer (JJA). On such a short timescale, physical drought is best represented by meteorological patterns of precipitation.

In the Climate Prediction Center's (CPC) percentile scheme, drought is defined as the number of consecutive days where a measured quantity (soil moisture or precipitation) is below a threshold (NDMC, 2008). Thresholds are derived from historical precipitation trends, and classified by severity. According to Burke et al. (2006), on average, 20% of the

global land surface is in drought. The CPC's threshold for moderate drought follows this assumption and assigns the threshold for moderate drought at the 20th precipitation percentile. Defining drought in this manner eliminates biases between models, observations and climate, and provides a simple, consistent method of drought persistence quantification. This study uses 20th precipitation percentiles calculated from historical precipitation records in IPCC models and observations to assess global drought persistence.

4.2 METHODS

Data

For the purpose of later comparison, analysis of 20th century drought employs the same suite of models and observations used in the previous chapter to assess land-atmosphere coupling. For the drought analysis, global data from the VIC model (VIC_GLOB) is used for model-observation comparison because it is the best estimate of global drought conditions and has been evaluated for its reproduction of large-scale drought (Sheffield and Wood, 2008).

Analysis

Twentieth precipitation percentiles were calculated using daily precipitation data reshaped into pentads, regridded to a 2°x2° grid and smoothed over 6°x6° boxes—in the same manner as the anomalies in the previous chapter. Twentieth precipitation percentiles were calculated for each summer pentad (19 summer pentads) by grouping the historical record (spanning 40 years or more) for the pentad of interest with the records of adjacent pentads creating a three-pentad "superset" to improve the sample size (superset=[pentad$_{i-1}$+

$pentad_i$+ $pentad_{i+1}$]). The precipitation values from all model years in the superset record were ranked by magnitude, and 20th precipitation percentiles calculated from the superset for each pentad of each model. Thresholds were used to determine the number of drought pentads for each model summer by comparing precipitation in each pentad to its corresponding threshold to classify each pentad in the model record as being in drought, or not in drought. Pentad drought data was then used to find the length of each summer drought, determined by the number of consecutive drought pentads.

From drought lengths, drought frequencies were generated for each model for three different focus regions (Great Plains, Sahel, northern India) to determine whether some models were more likely to exhibit longer droughts than others. Drought frequencies (Fr) were calculated by first determining the range in drought lengths (l) for each model, summing over the total number of droughts for each length in the model record and dividing by the number of decades in the record to normalize the distribution between models with different record lengths.

$$Fr(l) = \frac{\sum(drought\_length = l)}{\#\,decades} \qquad (7)$$

Because droughts do not occur in predictable or deterministic patterns, their stochasticity may also be mathematically analyzed and modeled (Dracup et al., 1980). A common stochastic model for precipitation is the two-state first order Markov chain described by Wilks (2006). This model is well suited for precipitation because there are only two possible states for the system, rain or no rain. In a first order Markov chain, transition probabilities govern the change from one state to another—these probabilities are only dependent upon the state of the previous member of the time series. The transition

probability of most interest in this case is the probability that a pentad in drought (pentad value=0 if in drought) will stay in drought, shown in (8).

$$P_{00} = \Pr\{Pentad_{t+1} = 0 \mid Pentad_t = 0\} \quad (8)$$

This transition value (P_{00}) may be directly calculated from the pentad drought data generated by the 20th percentile thresholds. For each spatial point in each model, summing all the drought pentads preceded by a drought pentad and dividing by the total number of pentads in drought computes a single P_{00} value. In a two-state model there are a total of four transition probabilities, but only two that need to be independently calculated because the four probabilities may be divided into two pairs that sum to one.

The other calculated transition probability is the probability that a pentad not in drought (pentad value=1 if not in drought) will be followed by a pentad in drought shown in (9).

$$P_{10} = \Pr\{Pentad_{t+1} = 0 \mid Pentad_t = 1\} \quad (9)$$

This transition probability (P_{10}) may be easily quantified in a method similar to P_{00}, however, error introduced by the edge effect of the summer pentad data series and the prescription of drought probability (20%) make it more preferable to calculate P_{10} from P_{00} as follows:

The probability that a pentad will be in drought is given by (10).

$$\Pr\{pentad_{t+1} = 0\} = P_{00} * \Pr\{pentad_t = 0\} + P_{10} * \Pr\{pentad_t = 1\} \quad (10)$$

By defining drought as the 20th percentile,

$$\Pr\{pentad_{t+1} = 0\} = \gamma = .20 \quad (11)$$

and therefore,

$$\Pr\{pentad_{t+1} = 1\} = (1 - \gamma) = (1 - .20) \quad (12)$$

Substituting (11) and (12) into (10) yields,

$$P_{10} = \left(\frac{.20}{1-.20}\right) * \left(1 - P_{00}\right) \qquad (13)$$

Using these transition probabilities, a first-order Markov dataset for each model may be generated using a random number generator. The utility of this randomly generated first-order Markov dataset is that a much longer time series than is available in either model or observational records may be created using the transition probabilities unique to each model. Figure 4.1 illustrates the simple if-statement loops used to generate Markov drought data for each IPCC model.

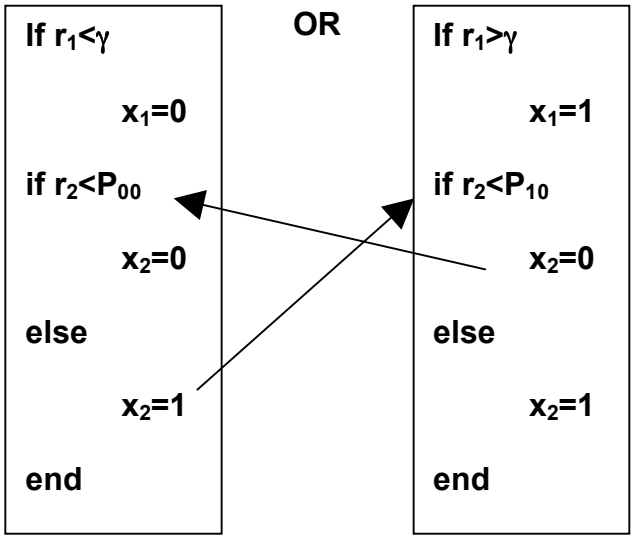

Fig. 4.1. *Generating Markov Drought Data: Given a drought threshold γ, a time series of randomly generated values between 0 and 1 called r (r has length=2 in the diagram), and values of P_{00} and P_{10} from the model, a Markov dataset called x of two-state variables (drought=0 or not drought=1) is generated using the looped set of if-statements depicted above.*

Markov drought data was created with the same number of years and pentads as the IPCC data it was modeled after, however data generation was repeated 10,000 times for each model in order to create a very large sample size. The purpose of this large sample size was to extract 95% confidence limits for the drought frequencies calculated from IPCC data. Results from these analyses follow in the next section.

4.3 RESULTS AND DISCUSSION

Results from drought analyses are shown in Figures 4.2-4.5. Maps of the 20th precipitation percentiles for each model are found in Figure 4.2, and for comparison, a summer precipitation climatology from the University of Delaware (UDel) from long-term monthly precipitation means from 1950-1999 (ESRL, 2008) is included as well. The models appear to be broadly consistent with the UDel climatology in the tropics where drought thresholds are high as expected since JJA is the rainy season for this region. There are, however, also meaningful differences. Over Saudi Arabia CNRM and CCSM3 exhibit larger thresholds than many of the other models, and larger than expected from the UDel climatology. In CCSM3, large precipitation thresholds over Saudi Arabia may be attributed to that model's western extension of the Asian monsoon over the Arabian Peninsula (Meehl et al., 2006). Asia and the Sahel are also problematic for many models, with significant variation in the patterns and magnitudes of thresholds. Figure 4.2 essentially presents a different view of the same data shown in Figure 3.7, but provides a clearer representation of the climate biases carried into drought analysis on models.

The transition probability P_{00}, here used as a measure of drought persistence, is similarly mapped in Figure 4.3, with mean P_{00} from VIC and NARR over North America included for comparison. The 15-model mean is also mapped in Figure 5.1b. The patterns of drought persistence exhibited by the North American observations depict strongest drought persistence across the western U.S. and Southwest, consistent with the work of Cook et al. (2007, 2004) and Seager et al. (2007). However, few models seem to accurately reproduce patterns seen from the observations. CNRM, GFDL and CCSM3 all demonstrate larger drought persistence than found in the observations. In CNRM and GFDL large drought

persistence spans the entire southern U.S., and in CCSM3 the entire Great Plains is the most

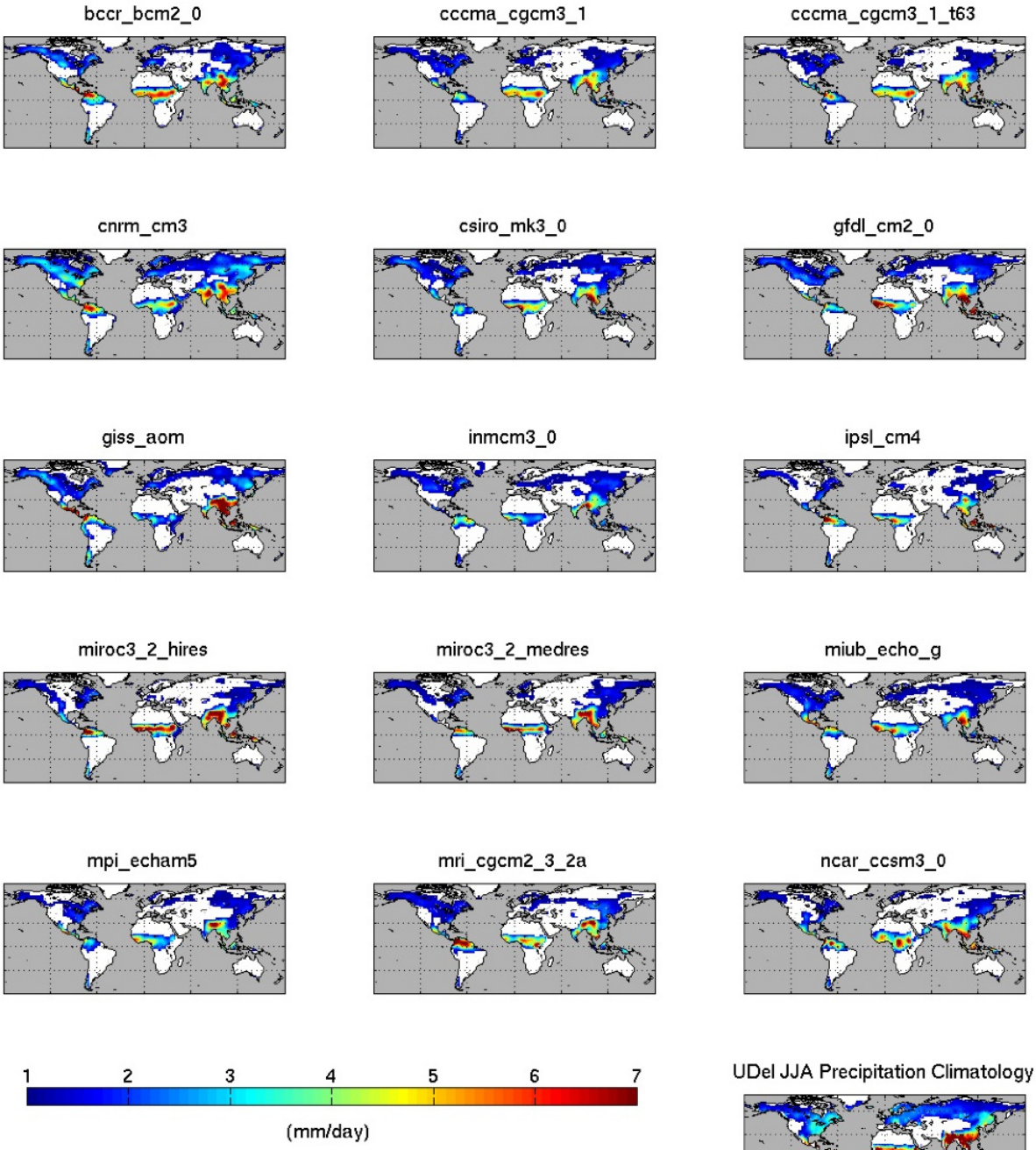

Fig. 4.2. *Average JJA 20th precipitation percentiles for 15 IPCC models, and JJA climatology from the University of Delaware (UDel) calculated from long-term (1950-1999) monthly means. Values < 1mm/day are omitted. Model thresholds are broadly consistent with climatological expectations that thresholds will be highest in the tropics where JJA is the rainy season, however there are significant inter-model differences as well, notably over Southeast Asia and the Sahel.*

drought prone region in North America. Between the models, there is a great deal of variation in the persistence of drought in the Sahara desert and southern equatorial Africa. MRI, IPSL, GISS, GFDL and CNRM models all exhibit large drought persistence over the

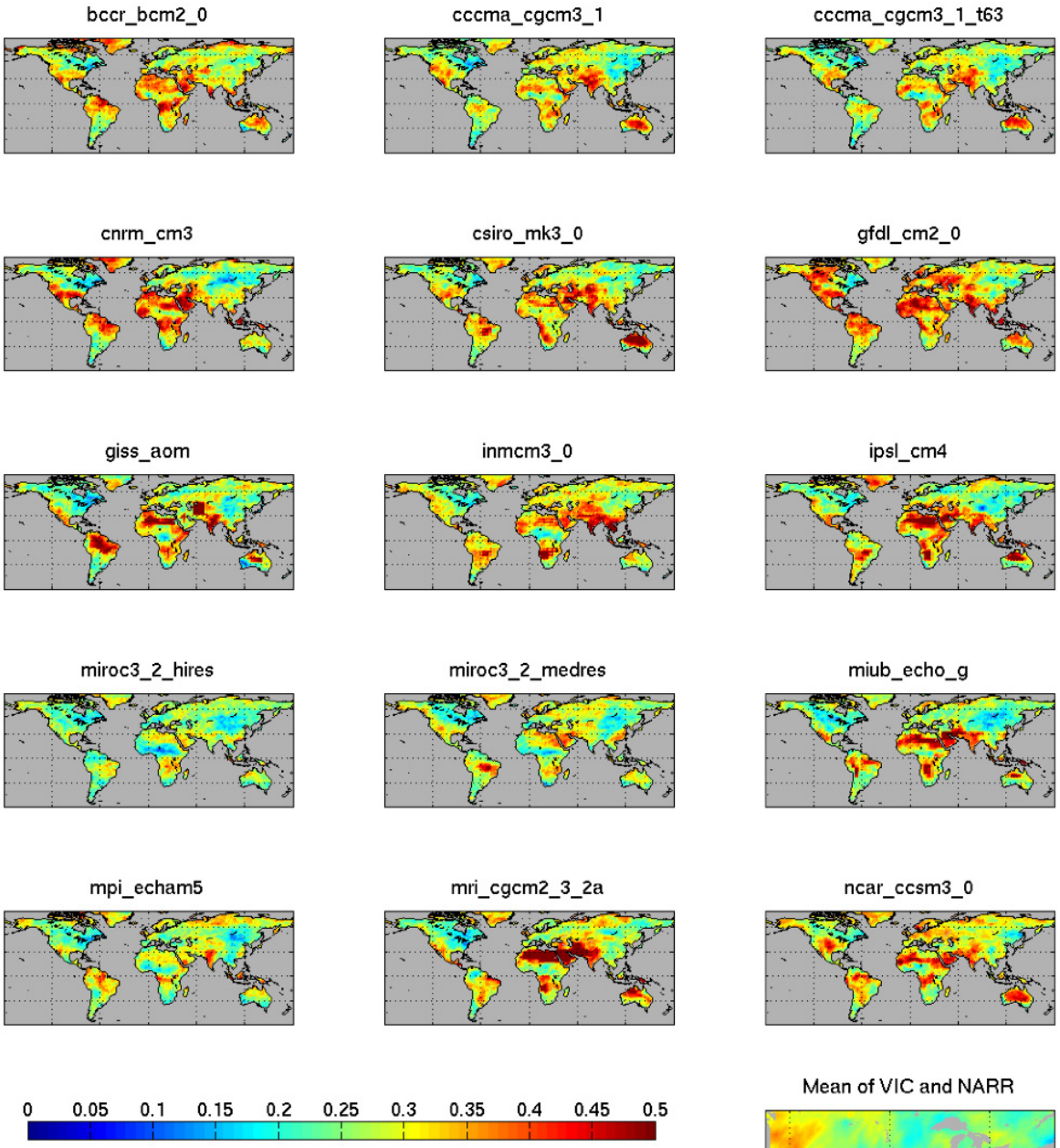

Fig. 4.3. *Drought persistence quantified by the two-state Markov chain's transition probability P_{00}, the probability that a pentad in drought will be followed by a pentad in drought. P_{00} values are mapped for 15 IPCC models. Also included is the NARR and VIC mean P_{00} over North America for model-observation comparison.*

Sahara with several of the models spreading persistence across Saudi Arabia and into southwestern Asia and India. Conversely, the MIROCh and ECHAM5 models show less drought persistence over North American than found in the observations, and globally, drought persistence is generally smaller than found in the other models. Few models recognize the Sahel as a region of particular drought persistence, a curious feature since the region was experiencing drought for several decades in the latter half of the 20th century (Narisma et al., 2007; Foley et al., 2003). Comparing Figures 3.7 and 4.3 illustrates that drought persistence is not directly related to departures in climatological precipitation. There do not appear to be any obvious connections between less than model average precipitation and high drought persistence or greater than model average precipitation and the absence of drought persistence.

Regions exhibiting extreme climatic behavior have been labeled "Hot Spots" in the literature. In Chapter 3, land-atmosphere coupling results were compared to the "Hot Spot" map of Koster et al. (2004). The term is applied non-uniformly to varying climatic features

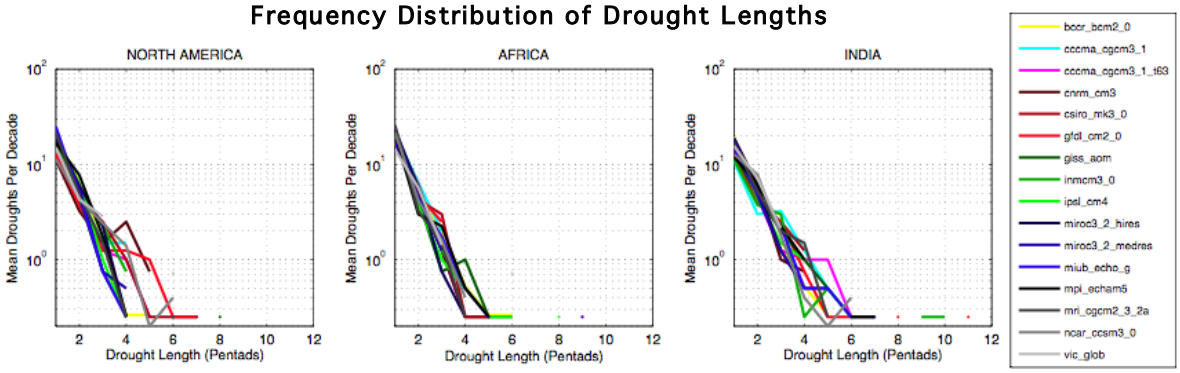

Fig. 4.4. *Drought frequencies for drought lengths calculated from 15 IPCC models and VIC_GLOB over the southern Great Plains in North America, the Sahel in Africa and northern India. Model probabilities appear to follow a somewhat linear trend (on a semi-log scale) for short droughts (3 pentads or less), at which point probabilities either go to zero, or depart for longer drought lengths. Model differences are most apparent in North America and India.*

and will not be used here. Instead, analysis is narrowed to three focus regions, previously introduced in Chapter 3. Drought length frequencies for the southern Great Plains in North America, the Sahel in Africa and northern India are shown in Figure 4.5. For all three locations, the occurrences of frequent short droughts (3-4 pentads or shorter) are fairly consistent among models. At drought lengths longer than 4 pentads, the model frequencies either go to zero—indicating there were no droughts of longer length in the model record, or depart from what was a mostly log-linear trend (some model's distributions become piece-wise after 8 pentads or more). Drought frequencies calculated from VIC_GLOB follow the former route, with no droughts in these regions greater than three pentads. Models appear broadly consistent with this observational data, however the 14-year record of VIC_GLOB is too short to make any behavior comparisons with great confidence. The reasonableness of model drought frequency behavior will be examined in detail later in this section.

In North America, CNRM, CSIRO, GFDL and CCSM3 exhibit larger frequencies for longer droughts and the longest drought lengths. A similar result is observed in India, where CGCM3t63, ECHO, GFDL, ECHAM5, and CCSM3 have the largest frequencies at longer drought lengths. Compared to the other regions, drought frequencies in the Sahel are in more agreement, with shorter droughts and smaller frequencies for longer ones. In North America and India the most persistent models had non-zero frequencies at droughts of six pentads or more. In Africa, only two models, BCM2 and IPSL, maintain log-linear frequencies to this length. Other curious behaviors of some models are the outlying values at large drought lengths. In North America, GISS has values for droughts of six and eight pentads, but none at five or seven. Difficult to see in the figure (better shown in Fig. 4.5) is that VIC_GLOB too, has an outlying value at six pentads, but none at four or five. In fact several models

exhibit this kind of behavior, suggesting that the solid probability line is indicative of the regions' inherent behavior, while the outliers represent a few uncharacteristically long drought events. This would certainly make sense in the Sahel. The IPSL and ECHO models extend to eight and nine pentad long droughts, such that for a few summers per decade in the models, half the summer season was in drought. The longest drought length found in the IPCC model data for the three regions examined lasted 11 pentads, occurred in northern India and was produced by the GFDL model.

Observations with much longer temporal record are required to make any definitive assessments regarding the validity of such long droughts in nature. However, datasets generated using the two-state Markov chain reproduce model behavior based on the persistence parameter calculated from the available model record and may be generated at much higher temporal resolution than their corresponding IPCC models. In this study, Markov datasets for each IPCC model were generated with 10,000 repetitions from which 95% confidence intervals for model drought frequencies were extracted. Figure 4.5 shows the drought frequencies seen in the North American plot of Figure 4.4, however each model is plotted individually with a confidence envelope. For the most part, drought length frequencies are contained within their confidence envelopes, with the exception of the outlying points that mostly remain outside the confidence intervals. This result is consistent with the hypothesis that the solid line of the frequency distribution is representative of inherent model behavior and outliers represent a few extreme events.

More importantly, Figure 4.5 affirms the theory that drought behaves primarily as a stochastic process. The two-state Markov chain model is a good fit for the data, such a good fit that there is no evidence of low frequency variability resulting from large scale

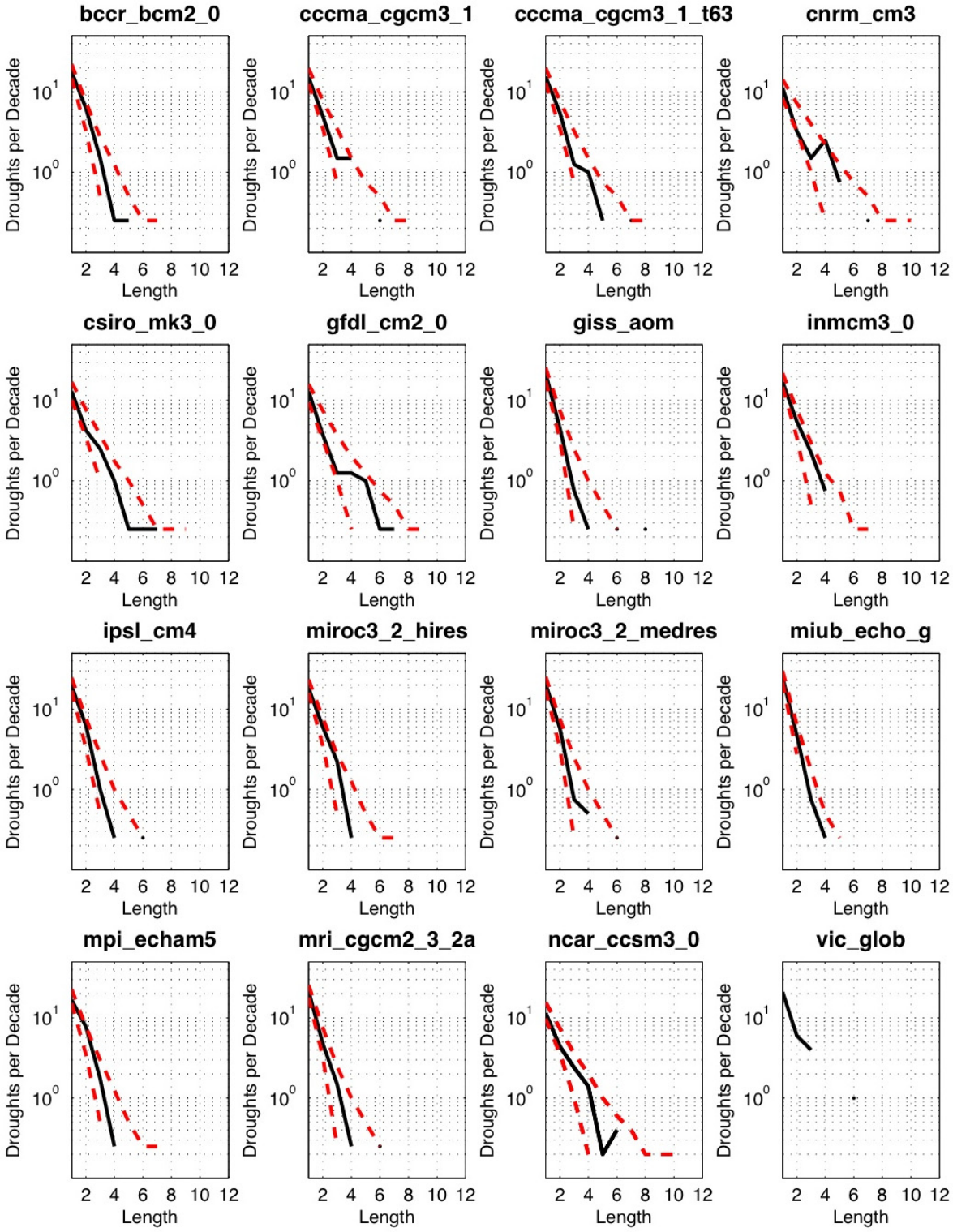

Fig. 4.5. *Drought frequencies of drought lengths for 15 IPCC models and VIC_GLOB (black) over the southern Great Plains and 95% confidence intervals (red) generated from Markov drought models (confidence limits for VIC_GLOB were omitted because of its short record). Again there is a great deal of spread among the models, however CSIRO, GFDL and CCSM3 appear to exhibit the longest droughts over this region, although several models (CGCM3, CNRM and GISS) have outliers at longer drought lengths.*

atmospheric processes suggesting that the signal from ENSO is not strong enough to make the statistics behave significantly different from a Markov process. Similarly, there is no evidence of bimodality, or climatic regime shifts at this intra-seasonal scale. Thus, the Markov drought model represents a significant result with practical applications for drought planning and risk assessment.

It is worth noting that one of the caveats of assessing drought persistence on an intra-seasonal scale using continuous drought pentads is seasonal cutoff eliminates the possibility for multi-year droughts as well as droughts that begin in the middle of a season and extend well into the next. As such, the close fit of the Markov model does not preclude the influence of ENSO or the existence of bimodality, which are both expected to be more important at longer, multi-year timescales. Intra-seasonal pentad drought analysis also limits comparability with drought studies using monthly time scales to evaluate drought persistence over annually continuous periods. For the purposes of this study, however, it was more relevant to calculate model drought persistence on a seasonal, pentad scale so that it could more appropriately be compared to the warm season land-atmosphere coupling calculated from the models, performed in Chapter 5.

CHAPTER FIVE: LAND-ATMOSPHERE COUPLING AND 20th CENTURY DROUGHT

5.1 THEORY

Model and observational analyses of the largest drought events in the 20th century have suggested that land-surface processes play a significant role in drought intensification and long-term maintenance (Sheffield and Wood, 2008; Rowell and Jones, 2006; Schubert et al., 2004a, 2004b; Narisma et al., 1997). Despite the apparent association between soil moisture feedbacks and precipitation variability (Schubert et al., 2004b; Narisma et al., 1997), the mechanisms that maintain or amplify drought are still not well understood. The goal of this analysis is to present a simple statistical method of quantifying land-atmosphere coupling strength, and use that metric to elucidate a connection between warm season land-atmosphere coupling and drought persistence. The emphasis of the analysis has been application of relatively simple statistical analyses to both model products and observational data. Here, that theme continues through analysis of the relationship between land-atmosphere coupling and drought persistence.

Consider the simplified hydrological model from Chapter 3.1 that exhibited no land-atmosphere coupling, and the threshold drought analysis from Chapter 4.1 defining the land surface to be in drought 20% of the time. Given this no-memory system, PE will be zero everywhere. Without precipitation memory, the probability of a pentad in drought being followed by a pentad in drought is just the probability of drought such that P_{00} is equivalent to P_0, or γ—the defined threshold for drought. Conversely, in a hydrologic model exhibiting near perfect precipitation memory, the limit of land-atmosphere coupling will go to one and if the initial state is drought, P_{00} will go to one as well. These two hypothetical hydrologic systems present extremes of the expected relationship between land-atmosphere coupling and

drought persistence. The anticipated result from these hypothetical hydrologic models is that GCMs with little or no land-atmosphere coupling strength will exhibit drought persistence near this study's 0.2 prescribed threshold, while drought persistence in models with large land-atmosphere coupling will—linearly or non-linearly—approach one as land-atmosphere coupling approaches one.

5.2 METHODS

Data

The analysis in this chapter compares the statistics derived in Chapters 3 and 4, and therefore employs the same IPCC models used in those chapters, listed in Table 3.1. In addition, this chapter includes analyses of all three sets of observational data: NARR, VIC_NA, VIC_GLOB.

Analysis

Analysis of land-atmosphere coupling and drought persistence engages the lag -2 cross-correlation of precipitation and evaporation, PE (described in detail in Chapter 3) and drought persistence parameter, P_{00} (described in detail in Chapter 4). The relationship between land-atmosphere coupling and drought persistence is calculated by plotting P_{00} against PE at lag -2 for all models and observations for the three focus regions. The magnitude of the linear correlation coefficient represents the association of land-atmosphere coupling and drought for models in that region. Results of this analysis are presented in the following section.

5.3 RESULTS AND DISCUSSION

Results of the land-atmosphere coupling and drought persistence analysis are presented in Figures 5.1 and 5.2. In Figure 5.1, the IPCC 15-model means of land-atmosphere coupling (PE correlation at lag -2) and drought persistence are mapped. The spatial patterns of these values have been discussed in previous chapters, however side-by-side maps of the model means are useful here to observe whether regions of strong land-atmosphere coupling broadly correspond with regions of large drought persistence. Visual inspection reveals that drought persistence does not exhibit the same type of localized "Hot Spot" distribution observed in land-atmosphere coupling. Drought persistence intensities span much larger spatial regions than that of strong land-atmosphere coupling. The areas of large land-atmosphere coupling do, however, tend to lie within the broader regions of large drought persistence. While no definitive conclusions may be drawn from such a visual inspection, these preliminary results appear to support the hypothesis that warm season land-atmosphere coupling contributes to warm season drought persistence in climate models.

A more quantitative connection between land-atmosphere coupling and drought persistence is presented in Figure 5.2 where drought persistence is plotted against land-atmosphere coupling for the three focus regions (southern Great Plains in North America, Sahel in Africa and northern India) considered in the previous two chapters. Numbers on plot axes correspond to the models listed in Table 3.1 with the addition of 16, 17 and 18 for VIC_GLOB, NARR and VIC_NA, respectively. Correlation coefficients for linear regressions are located in the bottom right of each plot. Of the three focus regions, the southern Great Plains depicts the strongest relationship (R=0.82) between drought

persistence and land-atmosphere coupling. Similar values—though not quite as large—are found in both the Sahel (R=0.80), and northern India (R=0.64).

This apparently linear relationship broadly agrees with our expectations from section

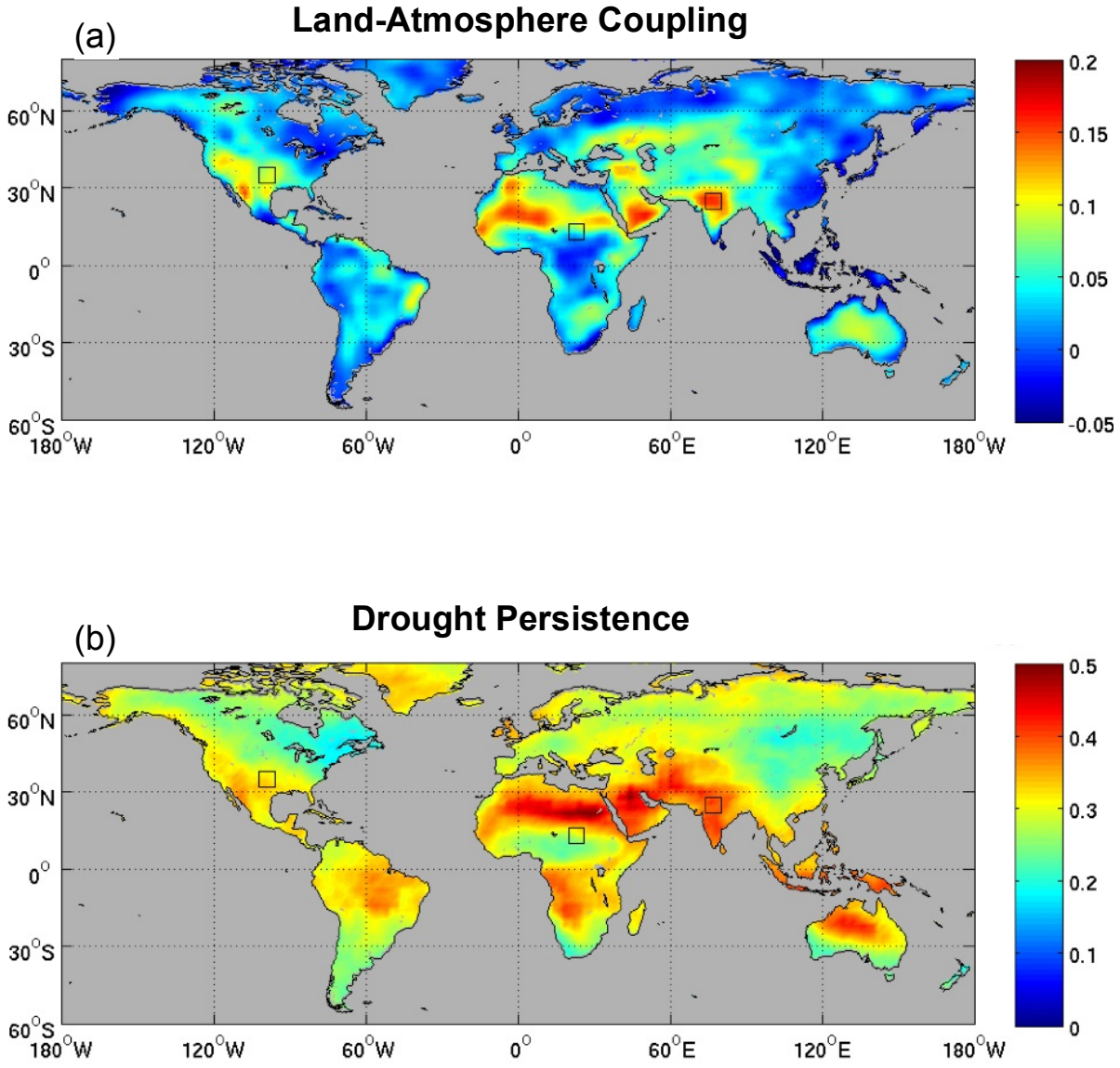

Fig. 5.1. *15-model means of warm season (JJA) (a) land-atmosphere coupling, measured as the lag -2 cross-correlation of precipitation and evaporation, and (b) drought persistence, from the Markov two-state transition probability, P_{00}. Drought persistence does not appear to exhibit the same kind of localized "Hot Spots" as land-atmosphere coupling. Instead, strong drought persistence spans much larger regions. However, Hot Spot locations appear to be contained within these broader areas of drought persistence.*

5.1, that models with little land-atmosphere coupling will have drought persistence close to the drought threshold, and drought persistence will increase with land-atmosphere coupling toward a limit of one. The distribution of models with large land-atmosphere coupling and large drought persistence is not constant among the three locations, however. In the Great Plains, the models at the upper end of the linear scatter are CNRM, CSIRO, GFDL and CCSM3. These models display more than twice the degree of land-atmosphere coupling, and one and a half times the drought persistence found in the NARR and VIC_NA observations—which fall along the lower end of the linear scatter. Interestingly, VIC_GLOB lies in the middle of the two. Disparities in the behaviors of the two VIC datasets are likely attributable to differences in record length (49 years for VIC_NA, 14 years for VIC_GLOB) and, to a lesser extent, model resolution (1° x 1° for VIC_NA, 2° x 2° for VIC_GLOB). Larger spatial resolution and temporal record in VIC_NA and its corroboration with NARR data lend it to be considered superior to VIC_GLOB in North America, however, the VIC_GLOB dataset is still considered the best global observational dataset available (Sheffield and Wood, 2008).

Regressions in the Sahel and northern India exhibit similar linear trends to that of the Great Plains, with notable differences. In the Sahel region, the linear scatter is more compressed; with generally lower land-atmosphere coupling and drought persistence than observed in the Great Plains. For example, models with large land-atmosphere coupling in the Sahel; BCM2, ECHO, GFDL and VIC_GLOB, have magnitudes comparable to models lying in the middle of the linear scatter of the Great Plains. Conversely, in northern India, models are more spread out with generally larger land-atmosphere coupling strengths than observed in the Great Plains. More models are found at the upper end of the linear scatter, in

this region and include CGCM3, CSIRO, GFDL, and INCM. In northern India, however, VIC_GLOB is clustered with the models at the lower end.

From section 5.1, the extreme values from a hypothetical hydrologic system with no land-atmosphere coupling and one with perfect land-atmosphere coupling could be two end-points of a line with slope 0.8 and y-intercept 0.2. Consider the linear fit to scatter plots in each of the three focus regions; the lines in North America and Africa are the best fit for the data with R^2 values of .68 and .64, respectively. Both lines also have y-intercepts near 0.2 (0.27 and 0.26, respectively) both slopes are smaller than the hypothetical model (0.68 and 0.57, respectively), yet their limits of P_{00} as PE approaches one are close to one (0.95 and 0.84, respectively). India displays the worst linear fit of the three regions with an R^2 of 0.40, y-intercept of 0.32 and slope of 0.40. Larger P_{00} when PE is small or zero indicates that there is some other memory source in this region contributing to the persistence of drought.

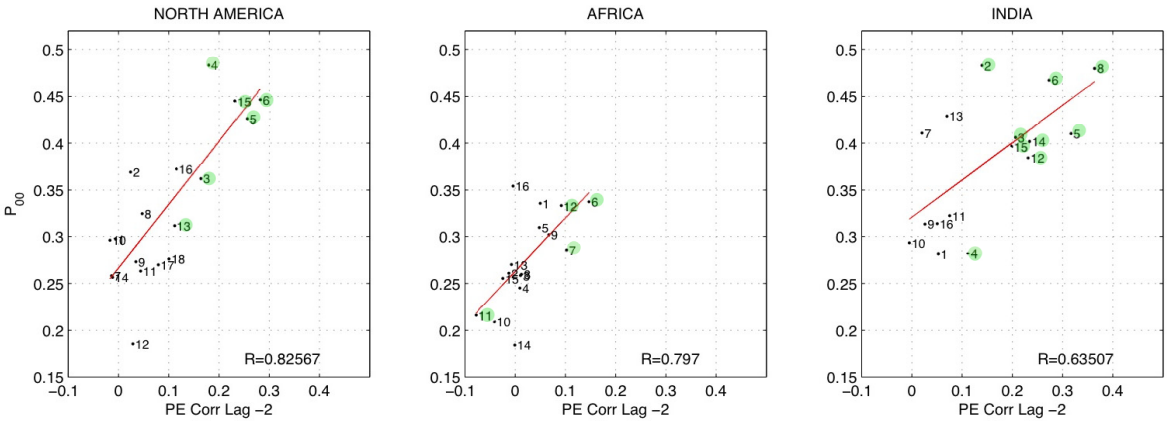

Fig. 5.2. *Linear regression of drought persistence (P_{00}) against land-atmosphere coupling (PE Corr Lag -2) for the southern Great Plains in North America, the Sahel in Africa and northern India, with correlation coefficients. Numbers correspond to models listed in Table 3.1, with the addition of 16, 17, and 18 for VIC_GLOB, NARR, and VIC_NA, respectively. Note that these figures include all values from all models. If only land-atmosphere coupling values significantly different from zero on a 95% confidence interval are included (highlighted in green), correlation values are 0.69 for six models in North America, 0.92 for four models in Africa, and 0.52 for nine models in India.*

Across the three focus regions, the GFDL model consistently exhibits large land-atmosphere coupling and drought persistence while the MIROCh and MIROCm consistently exhibit small land-atmosphere coupling and drought persistence relative to the model distributions. In North America, however, these smaller values are more consistent with observational data than GFDL, suggesting that at least in the southern Great Plains, GFDL over-represents the degree of land-atmosphere coupling found in observations and correspondingly exhibits larger than observed drought persistence—consistent with the findings of Ruiz-Barradas and Nigam (2006) that the GFDL model in North America exhibits much larger than observed precipitation recycling. Without global observations of longer temporal record, it is unwise to make similar assertions about the behavior of models relative to VIC_GLOB in the other regions. If conclusions *were* to be drawn for these other regions based on the behavior of VIC_GLOB, then climate models generally under-represent land-atmosphere coupling in the Sahel and over-represent it in northern India.

Results of these analyses show a linear relationship between warm season land-atmosphere coupling strength and drought persistence in IPCC climate models. These results confirm the hypothesis of this, and many other studies, that land-atmosphere feedbacks provide a mechanism for maintaining droughts. This is an important result for several reasons. First, it provides independent confirmation of the connection between land-surface feedbacks and drought maintenance. Second, awareness of the spread of model land-atmosphere coupling strength is useful when considering the reproducibility of drought statistics and individual events by climate models—that some models may severely over- or under-represent drought persistence compared to observations. For example, Schubert et al. (2004a) used the NSIPP model to reconstruct the 1930's Dustbowl and found that

interactions between the land-surface and the atmosphere increased the severity of the drought. However, Ruiz-Barradas and Nigam (2005) showed the NSIPP model exhibited more than four times the degree of local precipitation recycling as compared to observations, indicating that land-surface processes in the physical world may not be well-represented by the model. Third, an established relationship between land-atmosphere coupling and drought persistence may be a useful tool for forecasting the severity of future droughts in the presence of climate change. A linear relationship between drought persistence and land-atmosphere coupling provides a simple, physical basis for understanding why some models exhibit more drought persistence than others. Projections of future precipitation patterns suggest that dry areas will get drier as wet areas get wetter (IPCC, 2007a; Wentz et al., 2007). Feedbacks associated with strong land-atmosphere coupling are expected to amplify these hydrologic trends in the presence of climate change causing dry regions to become even drier than anticipated from shifting precipitation patterns alone. The relationship between land-atmosphere coupling in the 20th century and 21st century drought is analyzed in the next chapter.

CHAPTER SIX: 21st CENTURY DROUGHT

Model ensembles from future drought analyses, including the IPCC AR4, predict that climates in the future will be drier (see Fig. 1.1), yet the physics responsible for this drying are unclear. Individual models also exhibit a great deal of spread among future projections—thus, the ability to identify possible physical mechanisms responsible for departures in model behavior is important. The physical mechanism in question here, is whether land-atmosphere coupling in control simulations from the 20th century relate to changes in the hydrologic cycle in climate change simulations of the 21st century. The existence of such a relationship may provide valuable insight into the behavior of model hydrological cycles in future scenarios and narrow the spread among models.

6.1 THEORY

Analysis of warm season, 20th century drought in Chapter 4 assumed that on average, 20% of the land surface is in drought, thus prescribing drought frequency to be 20%. The purpose of examining future drought is to quantify the degree of change expected to occur relative to the present day base state; in this case the 20th century. Here, the degree of change is drought frequency; therefore the frequency of drought cannot be prescribed. Instead, analysis of warm season drought in the 21st century will use the same 20th precipitation percentile thresholds calculated from the 20th century to determine the effect increasing greenhouse gases will have on drought frequency relative to 20th century precipitation. Evidence of a transition to a more arid climate will manifest in this analysis through an increase in drought frequency, measured as the change in the number of pentads in drought each summer.

6.2 METHODS

Data

The PCMDI climate model data archive includes control runs for several scenarios of greenhouse gas emissions used in the IPCC's AR4. The scenario employed by this study is the Special Report on Emissions Scenarios A2 (SRES A2) (Nakicenovic et al., 2000). The SRES A2 scenario consists of yearly greenhouse gas and aerosol concentration values based on the assumption of a future world that is heterogeneous with continuously increasing population and regionally oriented economic growth that is more fragmented and slower than other emissions scenarios (Nakicenovic et al., 2000).

Daily precipitation data is available for 12 of the IPCC models used in this study, for two 20-year segments of the 21st century best compared to years 2046-2065 (mid-21st) and 2081-2100 (late-21st). The IPCC models used for future drought assessment include those listed in Table 3.1 minus CGCM3t63, GISS and MIROCh.

Analysis

21st century drought is calculated in the same manner as 20th century drought in Chapter 4.2, including the use of precipitation thresholds based on 20th century precipitation. Drought frequencies are calculated from the mean number of JJA pentads in drought. Changes in drought frequency representative of the entire model ensemble from the 20th and 21st centuries are calculated from the 12-model median of annual mean summer drought pentads. Changes in drought frequency between 20th and 21st centuries are calculated by differencing the median drought frequency of the mid- and late-21st with the median 20th century drought frequency.

6.3 RESULTS AND DISCUSSION

Results of 21st century drought analysis are presented in Figures 6.1 and 6.2. The map in Figure 6.1 shows the change in warm season drought frequency between the 20th century (20C3M) and the late-21st century (2081-2100) and histograms show the change in each model. Globally, most of the land surface experiences relatively little change in warm season drought frequency, however many of the largest increases are found in densely populated areas. The map shows large (20% or more) increases in drought frequency in the U.S.'s Pacific Northwest, Central America, central and northeast Brazil, Western and Eastern Europe, the western Sahel, the Mediterranean and southern Australia. Small (less than 10%) decreases in drought frequency are found in northwestern North America, Greenland, northwestern South America, the central Sahel and northern India. Change in drought frequency between the 20th and mid-21st centuries was also examined (not shown). Results exhibited the same regional drought frequency patterning found in the late-21st century but with smaller magnitudes of drought frequency change.

Global distributions of increasing drought frequencies broadly agree with other analysis of future drought. With the Hadley Centre's HadCM3 (not used in this study) SRES A2 GCM data and the PDSI, Burke et al. (2006) found that globally, the portion of the land surface in extreme drought would increase from 1% today, to 30% by the end of the 21st century and identified the U.S., Amazonia, Northern Africa, Southern Europe and Western Asia as likely to become drier. Sheffield and Wood (2008), using soil moisture from eight IPCC GCMs with two 20th century and three 21st century control experiments, including 20C3M and SRES A2, found model agreement that the Mediterranean, West Africa, Central Asia and Central America would experience more frequent long-term droughts in the 21st

century. In his RCCI Hot Spot analysis, Giorgi examined changes in interannual variability of precipitation and temperature between the 20th and 21st centuries for 20 IPCC GCMs using several future emissions scenarios including SRES A2. By his Hot Spot definition, Giorgi found that Central America, the Mediterranean and northeastern Europe emerged as the largest Hot Spots (see Fig. 2.4).

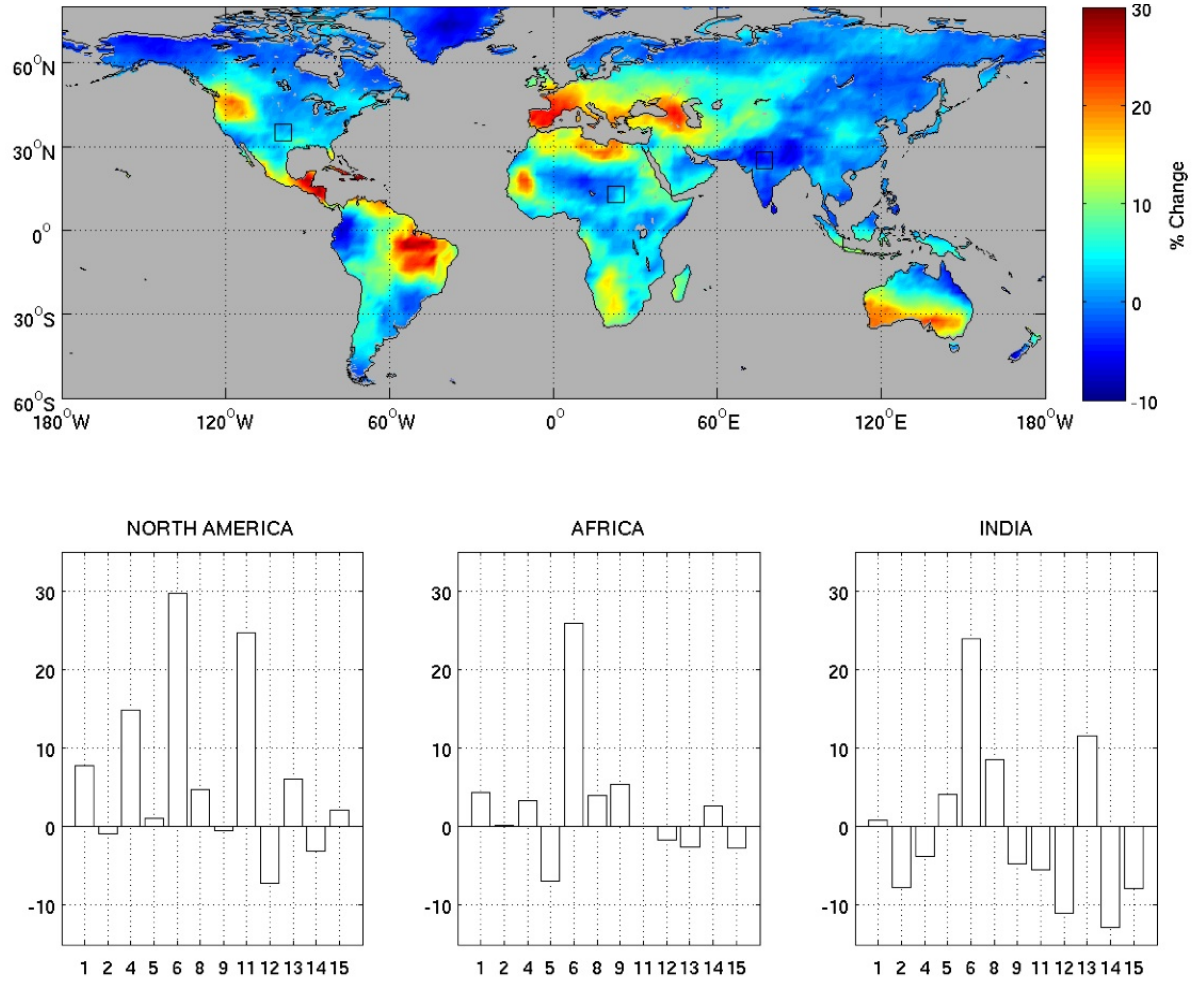

Fig. 6.1. *12-model median change in summer (JJA) drought frequency from the 20th century to the late-21st century (2081-2100). Histograms show change in drought frequency for each model from three focus regions in the southern Great Plains, Sahel and northern India. Numbers along the x-axis correspond to model numbers in Table 3.1, however note that 3, 7 and 10 are absent as these models were not available for the SRES A2 control run. Results from the late-21st century exhibit the same spatial patterns for drought frequency increase and decrease as the mid-21st century (not shown) but with greater magnitude.*

Drought patterns in Figure 6.1 are also consistent with the IPCC WGI expectations for future JJA precipitation patterns in Figure 1.1. The JJA maps in both figures show drying in the Pacific Northwest, Central America, northeast Brazil, Eastern and Western Europe, the Mediterranean, western Sahel and southern Africa. What Figure 1.1 also shows, however, is that DJF precipitation in the Pacific Northwest, and the Mediterranean increase, suggesting increased JJA drying may not prove to be as severe as it seems. The focus of this study is on boreal summer because it is most relevant to agricultural processes and when land-atmosphere coupling is expected to be most important (Koster et al., 2004).

A visual comparison of Figures 6.1 and 5.1 reveals no obvious connection between regions of strong land-atmosphere coupling or drought persistence in the 20th century and drought frequency in the 21st century. In fact none of the focus regions for land-atmosphere coupling emerge as regions with large increases in drought frequency. Further, warm season drought frequency in northern India decreases. This, at least might be physically explained by a faster warming of the land-surface in India compared to the sea surface, increasing the land-ocean temperature contrast, strengthening the summer monsoon and accounting for the increase in precipitation found over northern India.

Here again, models in each region exhibit large spread. The GFDL model, for example shows more than 20% increases in drought frequency everywhere. In North America, only the MIROCm model agrees with the sign and magnitude of change in drought frequency seen in the GFDL model, while in Africa a handful of models agree with the sign but none with even half the magnitude, and in northern India only four of the models agree with the sign of the change in drought frequency and none with the magnitude. Therefore,

compared to the ensemble model behavior, the GFDL model greatly over-estimates future drying in Africa and India, and possibly North America as well.

Figure 6.2 scatters the change in drought frequency between the 20th and mid- and late-21st centuries against both drought persistence (P_{00}) and land-atmosphere coupling (PE corr lag -2) for the focus regions. Unlike the linear relationship discovered between land-atmosphere coupling and drought persistence, there appears to be no connection between either drought persistence or land-atmosphere coupling in the 20th century and drought frequency in the 21st century. The cause of this result is not immediately apparent and needs further study thus the remainder of this discussion is largely speculative. It is conceivable, for instance, that warm season drought frequency in the future is controlled more by large-scale climate, and large-scale atmospheric circulation than local land-atmosphere coupling (Rowell and Jones, 2006).

It is also possible that changes in surface temperatures due to increasing greenhouse gases and global changes in precipitation patterns will incite climatic shifts such that dry regions get drier, wet regions get wetter and transition zones shift poleward (IPCC, 2007a, 2007b; Wentz et al., 2007; Seniveratne et al., 2006). If, as Koster suggested, strong land-atmosphere coupling is tied to semi-arid regions then geographical regions that exhibit strong land-atmosphere coupling in the 20th century may not exhibit strong land-atmosphere coupling in the 21st century with changes in regional climate. Gao and Giorgi (2008) found that the Mediterranean region would become increasingly arid in the 21st century and identified it as a region particularly vulnerable to the effects of climate change. Similarly, Seniveratne et al. (2006) found that climate regimes in Europe will shift northward in the 21st

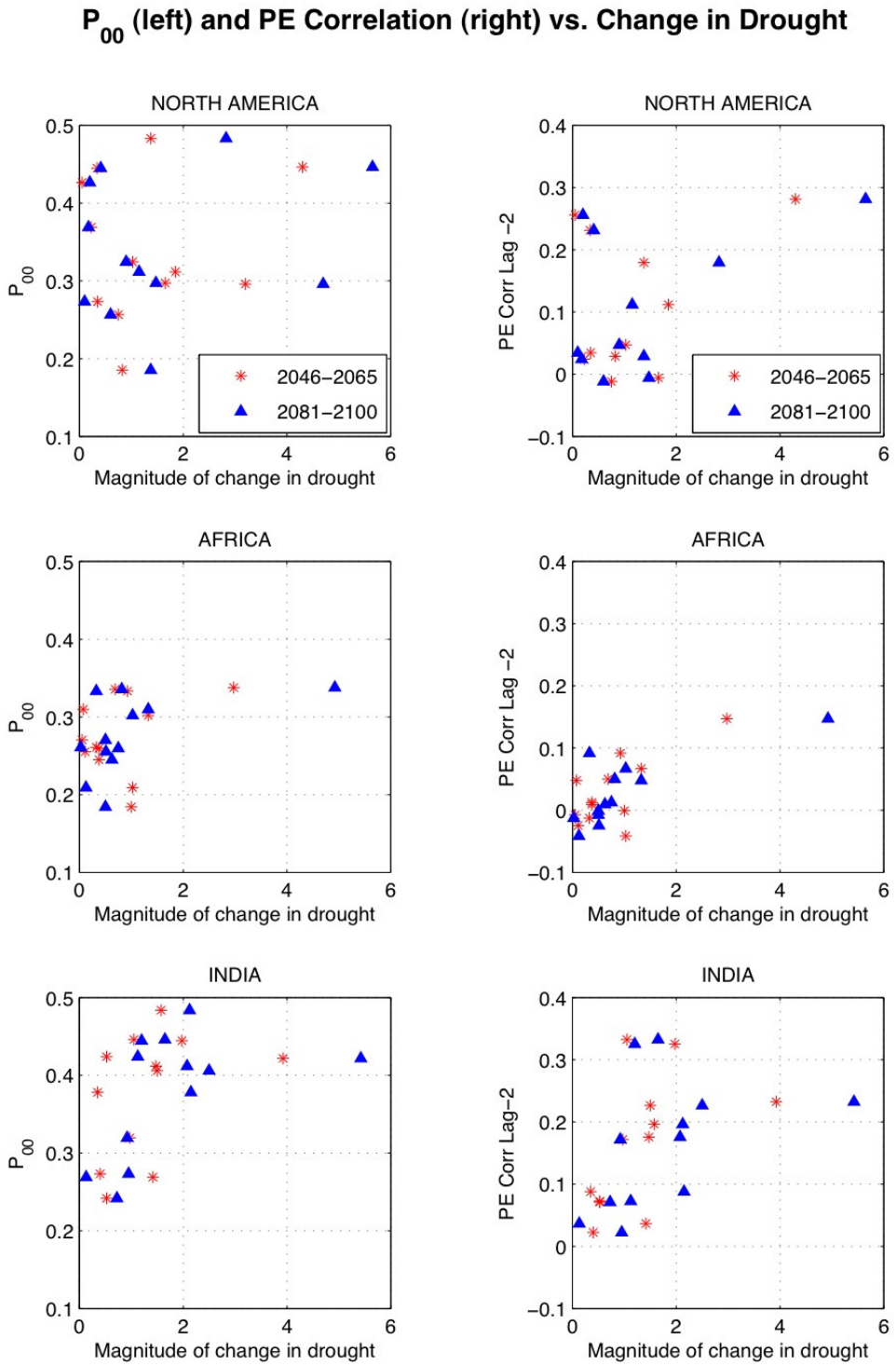

Fig. 6.2. *20th century drought persistence (P_{00}) and land-atmosphere coupling (PE corr lag -2) scattered against the change in drought frequency between the 20th and mid- and lat-21st centuries for 12 IPCC models. No apparent connection exists between drought frequency in the 21st century and land-atmosphere coupling or drought persistence in the 20th.*

century creating a new transition zone with corresponding large land-atmosphere coupling in central and Eastern Europe. The theory of northward shifting climate regimes is a subject for future study, but within the framework of this analysis, could be tested by repeating the calculations from Chapter 3 on IPCC data from the 21st century.

Many studies of current and future drought have emphasized the importance of land-atmosphere feedback controls on the maintenance and severity of drought. Sheffield and Wood (2008) proclaimed, "The potential for more droughts and of greater severity is a possibility compounded by positive feedbacks" while Rowell and Jones (2006) similarly asserted that although they are not the primary mechanism driving summer drying, positive feedbacks between precipitation and soil moisture "act to amplify the effects of the [drought] driver mechanisms, providing a notable secondary contribution to rainfall reduction." The results from this study therefore present an unexpected, yet important result. Contrary to the assertions and findings of other drought studies, local land-atmosphere processes appear to bear little importance in the frequency of future summer drying. This suggests that some other, non-local mechanisms are responsible for the patterns of future summer drying and studies should shift their focus away from land-atmosphere feedbacks and towards another possible mechanism to explain model behavior.

CHAPTER SEVEN: SUMMARY AND CONCLUSIONS

There is much uncertainty about what the future, in a world of climate change, will bring. Of particular concern to human welfare is how climate change will affect the frequency of natural disasters; including tropical cyclones, heat waves, flood and drought (IPCC, 2007a). Among all natural disasters, prolonged drought is one of the most devastating and costly due to its wide spatial extent and often long duration (Sheffield and Wood, 2008; Cook et al., 2007; Herweijer et al., 2007). The ability to reliably predict the geography, severity and frequency of future drought events would be extremely valuable to governments, municipalities and disaster relief agencies. However, the problem of forecasting future drought is complicated beyond the uncertainty of future precipitation because the physical mechanisms responsible for long-term maintenance are not well understood (Schubert et al., 2004b). The most emphasized physical mechanism in the literature is the contribution of land-atmosphere feedbacks (or land-atmosphere coupling) to precipitation variability (Narisma et al., 2007, Schubert et al., 2004a, 2004b; Trenberth et al., 1988), yet the relationships between land-atmosphere processes and climate variability have not been clearly identified.

Using products from GCMs and observations, this study employs statistical methods to quantify land-atmosphere coupling, drought frequency and drought persistence in model control simulations for the 20th century to determine the relationship between land-atmosphere coupling and drought within the context of models and observations. The result is then applied to control simulations for the 21st century to investigate claims from the literature, that land-atmosphere coupling will amplify the effects of climate change (Sheffield

and Wood, 2008). The central questions this study addresses are; 1.) Can a simple statistical method applied to model products be used to quantify global patterns of land-atmosphere coupling that broadly agree with more complex model experiments? 2.) Are regions of strong land-atmosphere coupling more likely to suffer droughts of long duration compared to other regions? 3.) Are climate models with large land-atmosphere coupling more likely to experience longer and more frequent droughts in response to climate change?

7.1 LAND-ATMOSPHERE COUPLING

Land-atmosphere coupling was quantified by the lagged correlation of precipitation anomalies with evaporation anomalies at a time lag of -2 pentads (10 days) such that evaporation is leading precipitation. Using this method, regions of strong land-atmosphere coupling broadly agree with results of other land-atmosphere coupling analyses (Koster et al., 2004), however as with other analyses, there is a fair amount of disagreement in individual model behavior. Regions of strong land-atmosphere coupling are identified by the GLACE experiment (Koster et al., 2006; Guo et al., 2006) are also found here, in the southern Great Plains of North America, the Sahel in Africa and northern India. Differences in methods and models used between this and other land-atmosphere coupling analyses suggest co-located regions of strong land-atmosphere coupling are robust within the models. The models found to globally exhibit the strongest land-atmosphere coupling were the CSIRO and GFDL models, while ECHAM5 and both MIROC models generally exhibited weak land-atmosphere coupling.

Notable differences between the results of this analysis and others are the emergence of the Sahara desert and Saudi Arabia as regions of particularly strong land-atmosphere

coupling. The large correlations identified in these regions may result from very small, yet highly correlated anomalies of precipitation and evaporation. Additionally, because precipitation may be amplified by moisture sources other than evaporation it is possible that some other source—such as the ocean—is responsible for the strong moisture feedbacks in these regions. Nevertheless, the employment of lagged pentad precipitation and evaporation anomalies presents a robust method for quantifying land-atmosphere coupling in broad agreement with results of more complex model experiments.

7.2 20th CENTURY DROUGHT PERSISTENCE

Drought analysis used the CPC's percentile scheme by prescribing the frequency of drought as the 20th precipitation percentile to calculate frequencies of droughts of different lengths and a drought persistence parameter based on a two-state Markov chain transition probability. Compared to observational data in North America, CNRM, GFDL and CCSM3 demonstrate larger than observed drought persistence while drought persistence is generally small in MIROCh and ECHAM5. Few models identify the Sahel as a region of strong drought persistence—a curious result considering the region spent several decades in the latter half of the 20th century in severe prolonged drought (Narisma et al., 2007), however this may be an artifact of short data timescales such that with two or three decades of a forty-year data set in drought, precipitation percentiles will be more representative of a drought state, rather than the mean climate. For the three focus regions, drought length frequencies are consistent among models for short droughts (3-4 pentads), and broadly consistent with observations—although the available global observations were of short duration and low spatial resolution such that little conclusion could be drawn in comparison.

To test the significance of model drought frequencies, drought behavior was analyzed as a stochastic process using a two-state Markov chain. The Markov model is a good fit for this intra-seasonal analysis, as there is no evidence of low frequency variability due to ENSO, indicating that at short time scales, the signal from ENSO is not strong enough to affect Markov drought statistics. Additionally, no evidence of bimodality or regime shifts is captured within the drought frequency distributions. Thus, on intra-seasonal timescales, the Markov model is a practical statistical tool that could be useful for drought planning and risk assessment.

7.3 LAND-ATMOSPHERE COUPLING AND 20th CENTURY DROUGHT

Model and observational analyses suggest that land-surface feedbacks play an important role in the maintenance of long-term drought, yet the physical mechanisms responsible for long-term drought maintenance are not well understood. The motivation for this entire study is to investigate the relationship between land-atmosphere coupling and drought persistence in climate models and observations to determine if models with strong land-atmosphere coupling are prone to more persistent drought.

The relationship between land-atmosphere coupling and drought persistence is quantified by plotting the drought persistence parameter (P_{00}) against land-atmosphere coupling (PE corr at lag -2). The result shows a linear relationship such that models with large land-atmosphere coupling exhibit large drought persistence and models with small land-atmosphere coupling exhibit small drought persistence. Between the three focus regions analyzed, however, the distributions of models with large land-atmosphere coupling are not consistent, and several of the models display much greater values than the observational data.

Among the three focus regions, the GFDL model consistently appears at the upper end of the linear scatter, while the two MIROC models are consistently on the lower end. Comparing model behavior with observational data in North America indicates that MIROCh and MIROCm are a closer match to the observations. Based on global observations with limited temporal record, models tend to under-represent land-atmosphere coupling in the Sahel and over-represent land-atmosphere coupling in northern India.

The linear relationship between IPCC model land-atmosphere coupling and drought persistence confirms the hypothesis that land-surface feedbacks are an important mechanism for the maintenance of long-term drought, and provides a physical basis for relating land-atmosphere coupling to drought persistence in both climate models and observations. This result is and important one, particularly relating to the forecast of future drought frequency and severity. Given the relationship between land-atmosphere coupling and drought persistence in the model control runs for the 20th century, we expect these effects to amplify the hydrological response to climate change in the 21st century, thereby enhancing the frequency and severity of droughts in the future.

7.4 21st CENTURY DROUGHT

Model ensembles in analyses of future drought, including the IPCC report, agree that the future climate will experience extensive drying, yet the physics responsible for this drying are unclear. In addition, the models also display a great deal of spread in their analyses of future climate change. This study has established a physical relationship between land-atmosphere coupling and drought persistence in model simulations of the 20th century. An important question is whether, and to what extent, land-atmosphere coupling strength in

20th century climate model simulations affects the hydrological response to climate change in model simulations of the 21st century, and if it does, how will rising temperatures and hydrological extremes from increased concentrations of greenhouse gases and aerosols affect the role of land-atmosphere coupling on drought persistence in the future. Establishing the existence of such a relationship would be extremely valuable for understanding and analyzing the hydrological behavior of models in future climate scenarios.

21st century drought frequencies were calculated relative to 20th century precipitation thresholds to determine the change in drought frequency quantified as the percentage of JJA summer pentads in drought. The change in drought frequency in model simulations for the 20th century (20C3M) and future scenarios (SRES A2) was taken as the difference between the median drought frequencies of the two model ensembles using the 20C3M thresholds.

The largest increases in drought frequency in the 21st century, based on the multi-model ensemble, occur in the Pacific Northwest of the U.S., Central America, northeast Brazil, Europe, the western Sahel, the Mediterranean and southern Australia. Patterns of increasing drought frequency are in agreement with IPCC AR4 projections for changes in future JJA precipitation patterns. No clear spatial correlation exists between land-atmosphere coupling in the 20th century and increasing drought frequency in the 21st. This is surprising considering the expectation of this and other studies that land-atmosphere feedbacks amplify the effects of climate drying. Additionally, one of the focus regions for land-atmosphere coupling experiences less frequent JJA drought in the future scenarios. Once again, models exhibit a large spread in their results, and again the GFDL model stands out by expecting the largest increases in drought frequency in all three focus regions, with much larger increases than almost any other model.

The absence of a strong relationship between land-atmosphere coupling in the 20th century and drought in the 21st suggests that in the future, warm season drought frequency is more affected by non-local large scale atmospheric circulation processes, than local land-atmosphere feedbacks. It is also possible, however, that climate change will incite vegetative regime shifts such that the semi-arid regions and transition zones—identified in the 20th century, as locations with large land-atmosphere coupling—will shift poleward (Seniveratne et al., 2006).

Though the result of this future drought analysis is somewhat surprising because of the expectation that land-atmosphere feedbacks would amplify drying induced by climate change, it is an important result nonetheless. The fact that land-atmosphere coupling in the 20th century is not related to drought frequency in the 21st century indicates that previous studies may have overestimated the importance of land-atmosphere coupling in determining the hydrological response to climate change.

7.5 CONCLUSIONS

This study conducted statistical analyses on climate models and observations to quantify land-atmosphere coupling and drought frequency and relate them based on 20th century control data. The result found a strong linear relationship among climate models such that models with strong land-atmosphere coupling tend to be more drought prone than models with small land-atmosphere coupling. Available observational data in North America and globally from a limited temporal record indicate that in several regions, models largely over-represent the degree of land-atmosphere coupling in observations and therefore over-represent drought persistence. This relationship presents a potentially powerful physical

mechanism to account for increased drying found in model runs with future emissions scenarios. Somewhat surprisingly, no strong relationship between land-atmosphere coupling in the 20th century and increasing drought frequency in the 21st century could be established, suggesting non-local climate mechanisms are more important for future drying than local land-surface feedbacks. Evidently, land-atmosphere coupling associated with intra-seasonal drought persistence in the previous century plays a secondary role in projections for the current one. The absence of evidence in this analysis to support drought-related amplification of land-atmosphere coupling due to climate change, suggests that in a climate change regime, local recycling processes are not as important as the large-scale atmospheric circulation (Chou et al., 2008; Held and Sodan, 2006). Subsequent analyses of future drought must therefore look in a new direction to determine what physical mechanisms—such as land-ocean temperature contrasts (Biasutti and Giannini, 2006; Hoerling and Kumar, 2003), changes in ENSO patterns and shifts in stormtracks (Lorenz and DeWeaver, 2007; IPCC, 2007a)—may be responsible for drought maintenance in the future.

REFERENCES

Alley, R.B., J. Marotzke, W.D. Nordhaus, J.T. Overpeck, D.M. Peteet, R.A. Pielke Jr., R.T. Pierrehumbert, P.B. Rhines, T.F. Stocker, L.D. Talley and J.M. Wallace, 2003. Abrupt Climate Change. *Science*, **299**, 2005-2010.

Balling, R.C. and P. Gober, 2007. Climate variability and Residential Water Use in the City of Phoenix, Arizona. *Journal of Applied Meteorology and Climatology,* **46**, 1130-1137.

Barnett, T.P. and D.W. Pierce, 2008. When Will Lake Mead go dry? *Water Resources Research*, **44**.

Biasutti, M. and A. Giannini, 2006. Robust Sahel drying in response to late 20th century forcings. *Geophysical Research Letters*, **33**.

Bonan, G.B. and S. Levis, 2006. Evaluating Aspects of the Community Land and Atmosphere Models (CLM3 and CAM3) Using a Dynamic Global Vegetation Model. *Journal of Climate*, **19**, 2290-2301.

Bretherton, C.S., M. Widman, V.P. Dymnikov, J.M. Wallace and I. Blade, 1999. The Effective Number of Spatial Degrees of Freedom of a Time-Varying Field. *Journal of Climate,* **12**, 1990-2009.

Burke, E.J. and S.J. Brown, 2008. Evaluating Uncertainties in the Projection of Future Drought. *Journal of Hydrometeorology*, **9**, 292-299.

Burke, E.J., S.J. Brown and N. Christidis, 2006. Modeling the Recent Evolution of Global Drought and Projections for the Twenty-First Century with the Hadley Centre Climate Model. *Journal of Hydrometeorology*, **7**, 1113-1125.

Chou, C., J.D. Neelin, C-A, Chen and J-Y Tu, 2008. Evaluating the "rich-get-richer" mechanism in tropical precipitation change under global warming. *Journal of Climate,* In Press.

Cook, E.R., R. Seager, M.A. Cane and D.W. Stahle, 2007. North American drought: Reconstructions, causes and consequences. *Earth-Science Reviews*, **81**, 93-134.

Cook, E.R., C.A. Woodhouse, C.M. Eakin, D.M. Meko and D.W. Stahle, 2004. Long-term Aridity Changes in the Western United States. *Science*, **306**, 1015-1018.

Dai, A., F. Giorgi and K.E. Trenberth, 1999. Observed and model-simulated diurnal cycles of precipitation over the contiguous United States. *Journal of Geophysical Research*,**104**, 6377-6402.

Dirmeyer, P.A., 2006. The Hydrologic Feedback Pathway for Land-Climate Coupling. *Journal of Hydrometeorology*, **7**, 857-867.

Dracup, J.A., K. Seong Lee and E.G. Paulson Jr., 1980. On the Definition of Droughts. *Water Resources Research*, **16**, 297-302.

Eltahir, E.A.B, 1998. A Soil-Moisture-Rainfall Feedback Mechanism: 1. Theory and Observations. *Water Resources Research*, **34**, 765-776.

ESRL, 2008. University of Delaware Air Temperature and Precipitation. *Earth System Research Laboratory: Physical Sciences Division*. http://www.cdc.noaa.gov/cdc/data.UDel_AirT_Precip.html

Foley, J.A., M.T. Coe, M. Scheffer and G. Wang, 2003. Regime Shifts in the Sahara and Sahel: Interactions between Ecological and Climatic Systems in Northern Africa. *Ecosystems*, **6**, 524-539.

Frankignoul, C., A. Czaja and B. L'Heveder, 1998. Air-Sea Feedback in the North Atlantic and Surface Boundary Conditions for Ocean Models. *Journal of Climate*, **11**, 2310-2324.

Gao, X. and F. Giorgi, 2008. Increased aridity in the Mediterranean region under greenhouse gas forcing estimated from high-resolution simulations with a regional climate model. *Global and Planetary Change,* **62**, 195-209.

Giorgi, F., 2006. Climate change hot-spots. *Geophysical Research Letters*, **33**.

Goodrich, G.B. and A.W. Ellis, 2006. Climatological Drought in Arizona: An Analysis of Indicators for Guiding the Governor's Drought Task Force. *The Professional Geographer*, **58**, 460-469.

Guo, Z., P.A. Dirmeyer, R.D. Koster, G. Bonan, E. Chan, P. Cox, C.T. Gordon, S. Kanae, E. Kowalczyk, D. Lawrence, P. Liu, C-H. Lu, S. Malyshev, B. McAvaney, J.L. McGregor, K. Mitchell, D. Mocko, T. Oki, K. Oleson, A. Pitman, Y.C. Sud, C.M. Taylor, D. Verseghy, R. Vasic, Y. Xue and T. Yamada, 2006. GLACE: The Global Land-Atmosphere Coupling Experiment. Part II: Analysis. *Journal of Hydrometeorology*, **7**, 611-625.

Hastenrath, S., A. Nicklis and L. Greischar, 1993. Atmospheric-Hydrospheric Mechanisms of Climate Anomalies in the Western Equatorial Indian Ocean. *Journal of Geophysical Research*, **98**, 20219-20235.

Held, I.M. and B.J. Soden, 2006. Robust Responses of the Hydrological Cycle to Global Warming. *Journal of Climate*, **19**, 5686-5699.

Herweijer, C., R. Seager, E.R. Cook and J. Emile-Geay, 1353. North American Droughts of the Last Millennium from a Gridded Network of Tree-Ring Data. *Journal of Climate*, **20**, 1353-1376.

Hoerling, M. and A. Kumar, 2003. The Perfect Ocean for Drought. *Science*, **299** , 691-694.

Hurrell, J.W., J.J. Hack, A.S. Phillips, J. Caron and J. Yin, 2006. The Dynamical Simulation of the Community Atmosphere Model Version 3 (CAM3). *Journal of Climate*, **19**, 2162-2183.

IPCC, 2007a: Summary for Policymakers. In: *Climate Change 2007: The Physical Science Basis. Contribution from Working Group I to the Fourth Assessment Report of the Intergovernmental Panel on Climate Change* [Solomon, S., D. Qin, M. Manning, Z. Chen, M. Marquis, K.B. Averyt, M. Tignor and H.L. Miller (eds.)]. Cambridge University Press, Cambridge, United Kingdom and New York, NY, USA.

IPCC, 2007b: Summary for Policymakers. In: *Climate Change 2007: Impacts, Adaptation and Vulnerability. Contribution of Working Group II to the Fourth Assessment Report of the Intergovernmental Panel on Climate Change,* M.L. Parry, O.F. Canziani, J.P. Palutikof, P.J. van der Linden and C.E. Hanson, eds., Cambridge University Press, Cambridge, U.K.

IPCC, 2007c: Climate Change 2007: The Physical Science Basis. Contribution of Working Group I to the Fourth Assessment Report of the Intergovernmental Panel on Climate Change [Solomon, S., D. Qin, M. Manning, Z. Chen, M. Marquis, K.B. Averyt, M. Tignor and H.L. Miller (eds.)]. Cambridge University Press, Cambridge, United Kingdom and New York, NY, USA, 996 pp.

Keyantash, J. and J.A. Dracup, 2004. An aggregate drought index: Assessing drought severity based on fluctuations in the hydrologic cycle and surface water storage. *Water Resources Research*, **40**.

Keyantash, J. and J.A. Dracup, 2002. The Quantification of Drought: An Evaluation of Drought Indices. *Bulletin of the American Meteorological Society*, 1167-1180.

Koster, R.D., P.A. Dirmeyer, Z. Guo, G. Bonan, E. Chan, P. Cox, C.T. Gordon, S. Kanae, E. Kowalczyk, D. Lawrence, P. Liu, C-H. Lu, S. Malyshev, B. McAvaney, K. Mitchell, D. Mocko, T. Oki, K. Oleson, A. Pitman, Y.C. Sud, C.M. Taylor, D. Verseghy, R. Vasic, Y. Xue and T. Yamada, 2004. Regions of Strong Coupling Between Soil Moisture and Precipitation. *Science*, **305**, 1138-1140.

Koster, R.D., P.A. Dirmeyer, A.N. Hahmann, R. Ijpelaar, L. Tyahla, P.Cox and M.J. Suarez, 2002. Comparing the Degree of Land-Atmosphere Interaction in Four Atmospheric General Circulation Models. *Journal of Hydrometeorology*, **3**, 363-375.

Koster, R.D., Z. Guo, P.A. Dirmeyer, G. Bonan, E. Chan, P. Cox, H. Davies, C.T. Gordon, S. Kanae, E. Kowalczyk, D. Lawrence, P. Liu, C-H. Lu, S. Malyshev, B. McAvaney, K. Mitchell, D. Mocko, T. Oki, K.W. Oleson, A. Pitman, Y.C. Sud, C.M. Taylor, D. Verseghy, R. Vasic, Y. Xue and T. Yamada, 2006. GLACE: The Global Land-Atmosphere Coupling Experiment. Part I: Overview. *Journal of Hydrometeorology*, **7**, 590-610.

Koster, R.D. and M.J. Suarez, 2004. Suggestions on the Observation Record of Land-Atmosphere Feedback Operating at Seasonal Time Scales. *Journal of Hydrometeorology*, **5**, 567-572.

Koster, R.D., M.J. Suarez, R.W. Higgins and H.M. Van den Dool, 2003. Observational evidence that soil moisture variations affect precipitation. *Geophysical Research Letters*, **30**.

Lawrence, D.M., P.E. Thornton, K.W. Oleson and G.B. Bonan, 2007. The Partitioning of Evapotranspiration into Transpiration, Soil Evaporation, and Canopy Evaporation in a GCM: Impacts on Land-Atmosphere Interaction. *Journal of Hydrometeorology*, **8**, 862-880.

Liu, Z., M. Notaro and J. Kutzbach, 2006. Assessing Global Vegetation-Climate Feedbacks from Observations. *Journal of Climate*, **19**, 787-814.

Lorenz, D.J. and E.T. DeWeaver, 2007. Response of the Extratropical Hydrological Cycle to Global Warming. *Journal of Climate*, **20**, 3470-3484.

Lorenz, D.J. and D.L. Hartmann, 2006. The Effect of the MJO on the North American Monsoon. *Journal of Climate*, **19**, 333-343.

Mahanama, S.P.P. and R.D. Koster, 2005. AGCM Biases in Evaporative Regime: Impacts on Soil Moisture Memory and Land-Atmosphere Feedback. *Journal of Hydrometeorology*, **6**, 656-669.

Mahanama, S.P.P. and R.D. Koster, 2003. Intercomparison of Soil Moisture Memory in Two Land Surface Models. *Journal of Hydrometeorology*, **4**, 1134-1146.

McKee, T.B., N.J., Doesken and J. Kleist, 1993. The Relationship of Drought Frequency and Duration to Time Scales. *Eighth Conference on Applied Climatology*.

Meehl, G. A., C. Covey, T. Delworth, M. Latif, B. McAvaney, J. F. B. Mitchell, R. J. Stouffer, and K. E. Taylor, 2007: The WCRP CMIP3 multi-model dataset: A new era in climate change research. *Bulletin of the American Meteorological Society*, **88**, 1383-1394.

Meehl, G.A., J.M. Arblaster, D.M. Lawrence, A. Seth, E.K. Schneider, B.P. Kirtman and D. Min, 2006. Monsoon regimes in the CCSM3. *Journal of Climate*, **19**, 2482-2495.

Mesinger, F., G. DiMego, E. Kalnay, K. Mitchell, P.C. Shafran, W. Ebisuzaki, D. Jovic, J.Woollen, E. Rogers, E.H. Berbery, M.B. Ek, Y. Fan, R. Grumbine, W. Higgins, H. Li, Y. Lin, G. Manikin, D. Parrish and W. Shei, 2006. North American Regional Reanalysis. *Bulletin of the American Meteorological Society*, 343-360.

Maurer, E.P., A.W. Wood, J.C. Adam and D.P. Lettenmaier, 2002. A Long-Term Hydrologically Based Dataset of land Surface Fluxes and States for the Coterminous United States. *Journal of Climate*, **15**, 3237-3251.

Nakicenovic, N., J. Alcamo, G. Davis, B. de Vries, J. Fenhann, S. Gaffin, K. Gregory, A. Grubler, T.Y. Jung, T. Kram, E.L. La Rovere, L. Michaelis, S. Mori, T. Morita, W. Pepper, H.M. Pitcher, L. Price, K. Riahi, A. Roehrl, H.H. Rogner, A. Sankovski, M. Schlesinger, P. Shukla, S.J. Smith, R. Swart, S. van Rooijen, N. Victor, Z. Dadi, (2000). Special Report on Emissions Scenarios: A Special Report of Working Group III of the Intergovernmental Panel on Climate Change, Cambridge University Press, Cambridge, U.K.

Narisma, G.T., J.A. Foley, R. Licker and N. Ramankutty, 2007. Abrupt changes in rainfall during the twentieth century. *Geophysical Research Letters*, **34**.

NDMC, 2008. Understanding and Defining Drought. National Climate Prediction Center. http://drought.unl.edu/whatis/concept.htm#operational

Nijssen, B., R. Schnur and D.P. Lettenmaier, 2001. Global Retrospective Estimation of Soil Moisture Using the Variable Infiltration Capacity Land Surface Model, 1980-93. *Journal of Climate*, **14**, 1790-1808.

Notaro, M., 2008. Statistical identification of global hot spots in soil moisture feedbacks among IPCC AR4 models. *Journal of Geophysical Research Letters*, **113**.

PCMDI, 2007. CMIP3 Climate Model Documentation, References, and Links. http://www-pcmdi.llnl.gov/ipcc/model_documentation/ipcc_model_documentation.php

Rowell, D.P. and R.G. Jones, 2006. Causes and uncertainty of future summer drying over Europe. *Climate Dynamics*, **27**, 281-299.

Ruiz-Barradas, A. and S. Nigam, 2006. IPCC's Twentieth-Century Climate Simulations: Varied Representations of North American Hydroclimate Variability. *Journal of Climate*, **19**, 4041-4058.

Ruiz-Barradas, A. and S. Nigam, 2005. Warm Season Rainfall Variability over the U.S. Great Plains in Observations, NCEP and ERA-40 Reanalysis, and NCAR and NASA Atmospheric Model Simulations. *Journal of Climate*, **18**, 1808-1830.

Salas, J.D., J.W. Delleur, V. Yevjevich and W.L. Lane, 1980. Applied Modeling of Hydrologic Time Series. *Water Resources Publication*.

Schubert, S.D., M.J. Suarez, P.J. Pegion, R.D. Koster and J.T. Bacmeister, 2004a. On the Cause of the 1930's Dust Bowl. *Science,* **303**, 1855-1859.

Schubert, S.D., M.J. Suarez, P.J. Pegion, R.D. Koster, and J.T. Bacmeister, 2004b. Causes of Long-Term Drought in the U.S. Great Plains. *Journal of Climate*, **17**, 485-503.

Seager, R., M. Ting, I. Held, Y. Kushnir, J. Lu, G. Vecchi, H.P. Huang, N. Harnik, A. Leetmaa, N.C. Lau, C. Li, J. Valez and N. Naik. 2007. Model Projections of an Imminent Transition to a More Arid Climate in Southwestern North America. *Science*, **316**, 1181-1184.

Seneviratne, S.L., D. Luthi, M. Litschi and C. Schar, 2006. Land-atmosphere coupling and climate change in Europe. *Nature*, **443**, 205-209.

Sheffield, J. and E.F. Wood, 2008. Projected changes in drought occurrence under future global warming from multi-model, multi-scenario, IPCC AR4 simulations. *Climate Dynamics*, **31**, 79-105.

Trenberth, K.E., G.W. Branstator and P.A. Arkin, 1988. Origins of the 1988 North American Drought. *Science*, **242**, 1640-1645.

USDA. 2004. Climate and Man: Part One. University Press of the Pacific.

Wentz, F., L. Ricciardulli, K. Hilburn and C. Mears, 2007. How much rain will global warming bring? *Science*, **317**, 233-235.

Wetherald, R.T. and S. Manabe, 2002. Simulation of hydrologic changes associated with global warming. *Journal of Geophysical Research*, **107**.

Wilks, D., 2006. Statistical Methods in the Atmospheric Sciences, 2nd Ed. Academic Press, Burlington, MA.

Wu, W. and R.E. Dickinson, 2005. Warm-season rainfall variability over the U.S. Great Plains and its correlation with evapotranspiration in a climate simulation. *Geophysical Research Letters,* **32**.

Zhang, X. and J.E. Walsh, 2006. Toward a Seasonally Ice-covered Arctic Ocean: Scenarios from the IPCC AR4 Model Simulations. *Journal of Climate*, **19,** 1730-1747.

Zhang, J., W-C Wang and J. Wei, 2008. Assessing land-atmosphere coupling using soil moisture from the Global Land Data Assimilation System and observational precipitation. *Journal of Geophysical Research,* **113**.

Zheng, X. and E.A.B. Eltahir, 1998. A Soil Moisture-Rainfall Feedback Mechanism: 2. Numerical Experiments. *Water Resources Research*, **34**, 777-785.